AN ABSTRACT OF THE THESIS OF

Lewis Gregory Hogan for the Doctor of Philosophy

in Physics presented on July 26, 1973

THE RECOMBINATION OF ATOMIC OXYGEN

Redacted for privacy

Abstract approved:

David S. Burch

The three-body heterogeneous and wall recombination coefficients for atomic oxygen were measured using an electron paramagnetic resonance spectrometer to monitor the time dependence of the atomic oxygen concentration. This measurement was made for a pressure range of from .224 to 1.10 torr using pyrolysis of ozone as a source of oxygen atoms. The three-body heterogeneous rate constant, k_1, with molecular oxygen as the third body was determined independent of ozone concentration to be $(5.43 \pm .08) \times 10^{-34}$ cc^2 · molecule^{-2}sec^{-1}. The wall recombination efficiency, γ, for a fused metaphosphoric acid-sodium metaphosphate mixture, the wall coating, was found to be 9.1×10^{-6}.

The recombination coefficient, k_1, resulting from a computer fit of the data to the usual recombination model is compared to literature values obtained from discharged oxygen, ozone pyrolysis, and chemiluminescence measurements.

The role that ozone concentration plays throughout the atomic oxygen decay and the possible effects of its neglect is discussed.

The Recombination of Atomic Oxygen

by

Lewis Gregory Hogan

A THESIS

submitted to

Oregon State University

in partial fulfillment of
the requirements for the
degree of

Doctor of Philosophy

June 1974

APPROVED:

Redacted for privacy

Professor of Physics in charge of major

Redacted for privacy

Chairman of Department of Physics

Redacted for privacy

Dean of Graduate School

Date of thesis presentation July 20, 1972

Typed by Suelynn Williams for Lewis Gregory Hogan

. . .

Then loudly cried the bold Sir Bedivere,
'Ah! my Lord Arthur, whither shall I go?
Where shall I hide my forehead and my eyes
For now I see the true old times are dead,
When every morning brought a noble chance,
And every chance brought out a noble knight.
Such times have been not since the light that led
The holy Elders with the gift of myrrh.
But now the whole ROUND TABLE is dissolved
And I, the last, go forth companionless,
And the days darken round me, and the years,
Among new men, strange faces, other minds.'

. . .

Alfred, Lord Tennyson

ACKNOWLEDGMENTS

The author would like to take this opportunity to thank all those people without whose help this work would not have been possible. He extends his gratitude to:

Dr. David S. Burch who not only suggested the experiment, but also spent many sleepless nights contemplating the data,

Dr. F. T. Lindstrom who suggested the computer fitting method,

Wade Meeker who not only helped with the glass blowing, but also listened to the author's oft-times impractical ideas, and

those many technicians from the Physics Shops who stopped their work to talk or fit my work into their schedule.

DEDICATION

To my wife, Joan, who may well
have been a widow,
To my children, Pat, Ann and John
who grew like orphans,
And to my parents who waited.

TABLE OF CONTENTS

TABLE OF CONTENTS CONTINUED

LIST OF TABLES

LIST OF FIGURES

THE RECOMBINATION OF ATOMIC OXYGEN

INTRODUCTION

Perhaps the most important nonphotolytic chemical reactions which occur in the upper atmosphere are those of the oxygen-ozone system

$$O + O_2 + M \rightarrow O_3 + M \qquad (1\text{-}1)$$

$$O + O_3 \rightarrow O_2 + O_2 \qquad (1\text{-}2)$$

$$O + O + M \rightarrow O_2 + M \qquad (1\text{-}3)$$

$$O_2(^1\Delta_g) + O_3 \rightarrow O_2 + O_2 + O \qquad (1\text{-}4)$$

where M represents a third body. It is these processes which influence the protective ozone layer in the stratosphere, and therefore make the rate constants for these reactions of great importance in chemical aeronomy. Recently, there has been much interest in these reactions and their role in smog production (40). These reaction rates are not known with much certainty and have been the object of much research in the past two decades.

Atomic Oxygen Recombination Measurements

There have been a number of methods used to investigate atomic oxygen recombination of which three will be discussed, one of which was used in the experiment which is the subject of this report. Most

atomic recombination measurements done prior to 1959 (2, 38, 27, 28) made use of metal probes which, when inserted into the system, measured by various schemes the energy lost by atoms recombining on the probe. These devices have several disadvantages (22): 1) They are slow in response, since the probe must be allowed to reach thermal equilibrium. 2) The accuracy is limited by the temperature measurement, and the fact that small variations in surface contamination of the probe can strongly affect the recombination rate. 3) The presence of the probe in the system can be a disturbing influence to the recombination being studied. One further disadvantage is that the probe cannot distinguish between recombining species.

A scheme which suffers few of these disadvantages employs nitrogen compounds and their reactions with atomic oxygen. One of the most sensitive methods for following O-atom recombination makes use of the air afterglow and NO titration (22). This procedure is based upon the fact that if a little nitric oxide is injected into a stream of O-atoms, the intensity, I, of the greenish-yellow air afterglow which is known to come from the reaction

$$O + NO \rightarrow NO_2 + h\nu \ ,$$

has been shown (21) to be proportional to the product $[O]\,[NO]$[1] and

---

[1] The square brackets enclosing atomic or molecular symbols signify concentrations.

is independent of the nature and amount of other gases present. This chemiluminescent reaction consumes NO and produces NO_2, but the [NO] is maintained constant by the fast and concomitant termolecular reaction

$$O + NO + M \rightarrow NO_2 + M,$$

and the extremely fast reaction

$$O + NO_2 \rightarrow NO + O_2 ,$$

which, in turn, destroys any NO_2 produced. Thus, if the light intensity is measured as a function of distance down a flow tube from the place where the NO is injected, and if the flow velocity, v, is known, then

$$\frac{d[O]}{dt} = v \frac{d[O]}{dx} \sim c \frac{dI}{dx} .$$

Much work has been done using this and variations of this technique (23, 32, 24, 36) which gives good results in spite of the following disadvantages: 1) The measured intensity of the afterglow may be seriously affected by axial and radial diffusion, viscous pressure drop (22), and the poor mixing of the injected NO unless special precautions are taken to minimize these effects. 2) Back diffusion is minimized by large flow velocities, but at the expense of increased uncertainty in the measurement of v, which is difficult to measure with much accuracy in any case. 3) To be able to determine the order of these

reactions, it is necessary to observe the rate of loss of oxygen atoms over several decay constants, and with fast flow systems this isn't possible. 4) Although there is some evidence to the contrary (21), the addition of nitrogenous impurities into the system to be studied has the possibility of altering the reaction rate under investigation. Although these difficulties may be minimized, they cannot be overcome totally.

The method for observing O-atoms which is used in the experiment to be discussed in this thesis and which suffers from the least experimental difficulties is Electron Paramagnetic Resonance[2], a technique which may be used for any species which has a magnetic or electric dipole moment. In using EPR to study recombination, one may proceed as in the foregoing method and observe the loss of free atoms down a flow tube, or measure directly a quantity which is proportional to $\frac{d[O]}{dt}$ by isolating the source of atoms from the detector at a designated time and observing the consequent decrease of concentration. If the former is used, then this technique suffers from the same problems as titration, ascertaining the flow velocity and measurement of the recombination over several decay constants. If the second method is employed, the chief experimental problems are the fabrication of a rapid valve which isolates the detector from the

---

[2]Hereafter designated as EPR.

atom source, the suppression of wall recombination, and the determination of the pressure at the detector, which is also a problem in all fast flow systems.

The two most common methods for measuring atomic oxygen concentrations in use at the present time are probably the air afterglow technique with its several variations and EPR. Westenberg and de Haas (44) have compared the results using both methods and find them to be in agreement to about 5%.

RECOMBINATION MECHANISMS

In order to decide which of the possible oxygen reactions are likely under the experimental conditions of the laboratory, we will consider the possible combinations of the three components most likely making up an atomic oxygen source; O, O_2, and O_3, in the ground or excited states. The reactions may be further divided into four groups: 1) two body wall recombinations, 2) three body wall recombinations, 3) volume recombinations, and 4) higher order complexes. These reactions are listed in Table I.

Two Body Wall Recombination

Under this heading are classed reactions of the following types:

$$O + O \cdot S \rightarrow O_2 ,$$

$$O + O_2 \cdot S \rightarrow O_3 ,$$

$$O + O_3 \cdot S \rightarrow 2O_2 ,$$

etc., where the symbol $O_n \cdot S$ signifies an O_n molecule adsorbed on the wall. The rate equation for these reactions is written as

$$\frac{d[O]}{dt} = - K_1[O][O] - K_2[O][O_2] - K_3[O][O_3] - \ldots ,$$

which may be simplified as

$$\frac{d[O]}{dt} = - [O]\{K_1[O] + K_2[O_2] + K_3[O_3] + \ldots\} .$$

Table I

Possible Mechanisms for Atomic Oxygen Recombination

Name	Mechanism
Two Body Wall	$O + O \cdot S \rightarrow O_2$
	$O + O_2 \cdot S \rightarrow O_3$
	$O + O_3 \cdot S \rightarrow 2\,O_2$
	etc.
Three Body Wall	$O + O + S \rightarrow O_2 + S$
	$O + O_2 + S \rightarrow O_3 + S$
Volume	$O + O \rightarrow O_2 + h\nu$
	$O + O + M \rightarrow O_2 + M$
	$O + O_2 \rightarrow O_3 + h\nu$
	$O + O_2 + M \rightarrow O_3 + M$
	$O + O_3 \rightarrow 2\,O_2$
	$O_2^* + O_3 \rightarrow 2\,O_2 + O$
	where M is any of the constituents O, O_2, O_3.
Higher Order Complexes	$O_2 + O_2 \rightarrow O_4$
	$O_2^* + O_2^* \rightarrow O_4^*$
	etc.

Now experimental evidence (27, 28, 14) demonstrates that oxygen atoms recombining on surfaces follow first order kinetics which implies that the quantity in braces is a constant. The Mechanism proposed by Greaves and Linnett (14) for O-atoms describes the recombination as taking place between an atom loosely bound to the surface and one from the volume, followed by the rapid replacement of the atom on the surface. The combination of O-atoms with an O_n molecule is probably similar, so that after the walls become saturated with molecules, the adsorbed gas remains nearly constant over a large span of pressures. Thus we write one equation representing this effect of walls as

$$\frac{d[O]}{dt} = - k_w[O] ,$$

where

$$k_w = \{K_1[O] + K_2[O_2] + K_3[O_3] + \dots \}.$$

Three Body Wall Recombination

In most cases of recombination the constituents approach each other under the influence of a mutual attraction with some relative kinetic energy. The total energy of such a system is positive, so that recombination can take place only if the system loses part of the kinetic energy and drops into a bound state during the time interval that the system is within the range of the potential. It is possible for the wall to act as a third body to remove this energy. At room

temperature the duration of the interaction is of the order of a vibration period, approximately 10^{-13} seconds. Since the average speed of a molecule at room temperature is of the order of 10^{4} cm/sec, only those two-body interactions which occur within 10^{-9} cm of the wall can also collide with the wall during the interaction time. In order to determine the degree to which walls play a role in three-body recombination, the ratio of three-body volume interactions to wall collisions will be estimated.

The number of three-body wall collisions which occur within an interaction time τ may be expressed as

$$\tfrac{1}{4} n' \bar{v} \tau A$$

where n' represents the concentration of two-body complexes, $\bar{v}$, the average speed of a molecule, and A, the surface area of the enclosure. Concomitantly, the number of termolecular volume interactions is given by the product

$$n' \tau Z V$$

where V designates the volume enclosed by the area A, $Z = \sigma n \bar{v}$, the collision frequency, with the quantities σ and n defined respectively as the collision cross section of a molecule with a two-body complex and the molecular concentration. σ will be of the order of the geometrical O_2 - O_2 cross section. Thus the desired ratio is given by

$$4\sigma\, n\frac{V}{A} \simeq 500 \frac{p}{\text{cm torr}} \frac{V}{A}$$

which shows that at one torr for enclosures of a reasonable size, the wall is ineffective as a third body compared to the volume recombination.

Volume Recombination

The recombination processes which occur in the volume of the reaction vessel may be categorized as two-body radiative, three-body volume, and neutral rearrangement recombinations. In the two-body process the system must radiate according to the Frank-Condon principle during the time of association from the region of the classical turning point to a vibrational level in some state of lower energy whose turning point is nearly directly below. Thus the number of recombinations that take place is determined not only by the collision time, but also by the radiative lifetime of the state along whose potential the two bodies associate. For states whose lifetimes are of the order of 10^{-8} sec, the previous consideration predicts approximately 10^{5} collisions before recombination may take place by this means. However, not all states within which the collisions take place are radiatively coupled to lower states so that the number of encounters necessary for recombination may be much higher.

The product $(\tau Z)^{-1}$ gives the fractional number of two-body

encounters that are also three-body collisions which at one torr pressure is 10^6 to one, so that at approximately ten torr, the three-body and radiative processes takes place at an equal rate. However, the number of radiative recombinations depends upon the lifetime of the electronic state along whose potential the two constituents approach. There are two three-body recombination reactions which are also radiatively possible. These are

$$O + O \rightarrow O_2 + h\nu, \quad O + O + M \rightarrow O_2 + M ;$$

$$O + O_2 \rightarrow O_3 + h\nu , \quad O + O_2 + M \rightarrow O_3 + M .$$

The first pair involves two oxygen atoms in the ground state which in order to recombine radiatively, must approach each other along either an excited state potential curve or that of the molecular ground state. All the molecular excited states formed from two $O(^3P)$ atoms are metastable with respect to radiation to the molecular ground state so that the lifetimes of those states are far in excess of 10^{-8} seconds. This result leads to a negligible probability for radiative recombination compared to the three-body process. The probability that radiative recombination will take place from some vibrational level in the molecular ground state is also insignificant since the transition probability for removal of energy by a vibrational transition is much smaller than that for electronic transitions (18, p. 401). For homonuclear molecules this transition probability

virtually vanishes (18, p. 80).

The second pair of reactions shown above represents the recombination of O and O_2 to form O_3. Since the potential curves and lifetimes of the excited states of ozone aren't well known, one cannot use the lifetime arguments that were made for the honogeneous combination to completely rule out the radiative recombination of O and O_2. However, the data from thermal decomposition studies of ozone (4, 46) are adequately explained without using the radiative process. This mechanism will be omitted from any model used to describe oxygen recombination in this experiment and to interpret the data.

In recent years it has been determined (23, 3) that if the excited metastable $^1\Delta_g$ and $^1\Sigma_g$ states of molecular oxygen are present, the reaction

$$O_2^* + O_3 \rightarrow O_2 + O_2 + O$$

where O_2^* is either of the metastable states, is a production mechanism for atomic oxygen and must be considered in any recombination model. Along with these neutral rearrangement reactions with deexcitation, there is the rearrangement process

$$O + O_3 \rightarrow O_2 + O_2$$

which completes the list of possible recombination processes except for higher order type phenomena.

Higher Order Complexes

There is little experimental evidence for the existence of complexes except that Bader and Ogryzlo (3) explain emission spectra from a mixture of $O_2(^1\Delta_g)$ and $O_2(^1\Sigma_g)$ as resulting from radiative dissociation of $O_4(^1\Delta_g, {}^1\Sigma_g)$ complexes. These mechanisms will be neglected in any model discussed for atomic oxygen recombination.

From the discussion above, it seems likely that the probable reactions are two-body wall, three-body volume, and neutral rearrangement. These are listed in Table II.

Table II

Probable Reactions for Atomic Oxygen Recombination

Name	Reaction	
Wall	$O + O\cdot S \rightarrow O_2$	(2-1)
Volume	$O + O + M \rightarrow O_2 + M$	(2-2)
	$O + O_2 + M \rightarrow O_3 + M$	(2-3)
	$O + O_3 \rightarrow O_2 + O_2$	(2-4)
	$O_2^* + O_3 \rightarrow O + O_2 + O_2$	(2-5)
	where M is any third body and O_2^* refers to O_2 in either the $^1\Delta_g$ or the $^1\Sigma_g$ state.	

ELECTRON PARAMAGNETIC RESONANCE THEORY

In this section only those features of EPR which aid in the understanding of the spectrum of atomic oxygen, the measurement of concentrations of O-atoms, and the determination of the concentration of $O_2(^1\Delta_g)$ relative to that of oxygen atoms will be discussed.

Electron Paramagnetic Resonance Theory of Atomic Oxygen

There are three naturally occurring isotopes of oxygen; O^{16}, O^{18} both have a nuclear spin of zero, and O^{17} has a nuclear spin of 5/2. An energy level diagram of O^{16}, the principal isotope, is shown in column a) of Figure 1. The ground state of atomic oxygen is $^3P_2$, which lies 158.5 cm^{-1} below $^3P_1$ and 226.5 cm^{-1} below $^3P_0$. In addition to the ^3P states, the ^1D and ^1S states lie 15,867.7 cm^{-1} and 33,792.4 cm^{-1}, respectively, above the ground state.

The effect of a magnetic field upon the ^3P energy levels of the oxygen atom has been calculated by Abragam and Van Vleck (1) to second order in H, the magnetic field; this calculation gives an accuracy to one part in 10^6 since terms of third order in H vanish for a ^3P term in L S coupling (35). Column b) of Figure 1 shows the multiplet splitting of the ^3P states due to the spin-orbit interaction while column c) indicates the linear Zeeman effect, which splits each multiplet into 2J + 1 equally spaced energy levels. In the last column, d), is shown the result of the quadratic Zeeman effect upon the levels

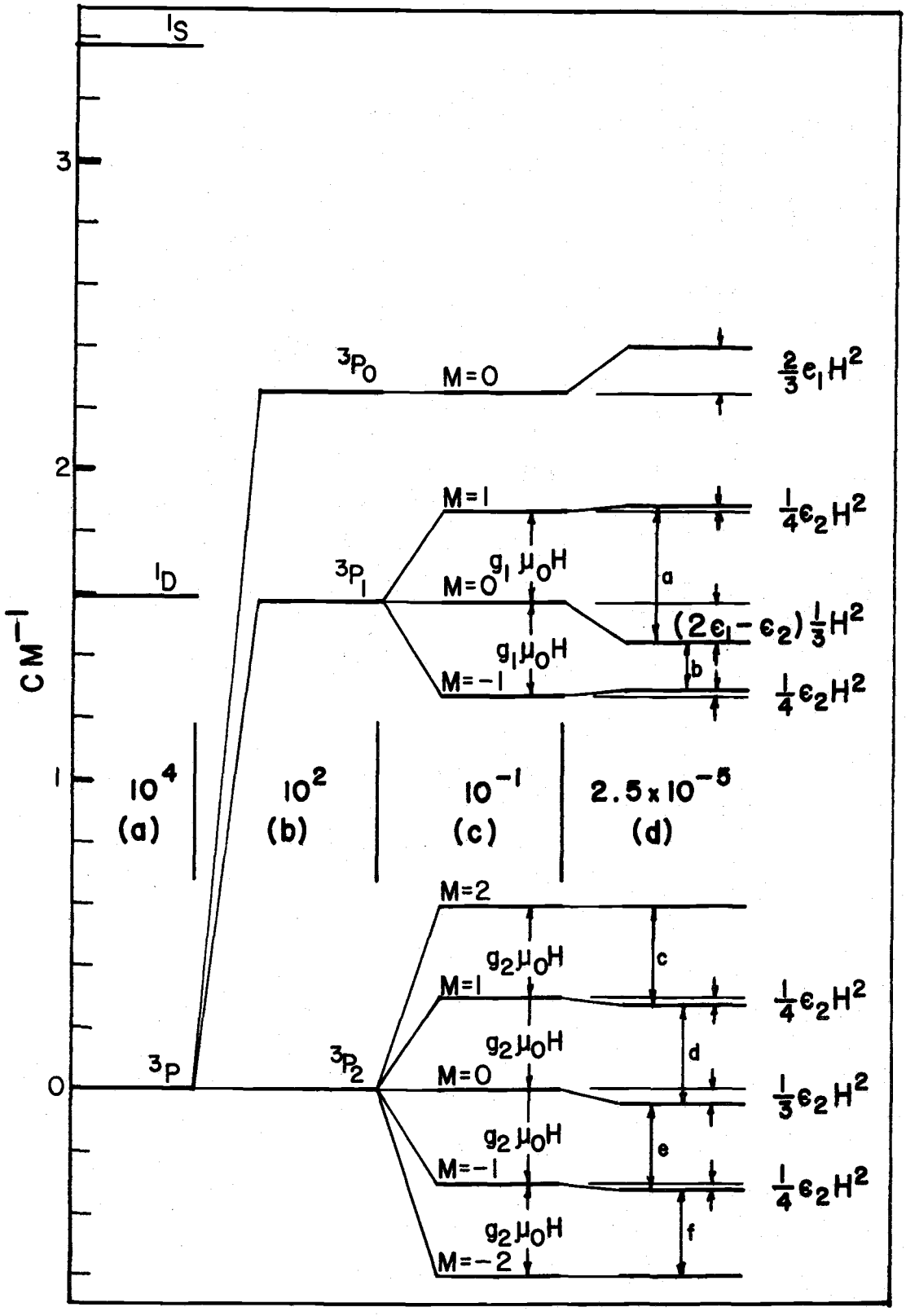

Figure 1. Energy level diagram for atomic oxygen in which ε_1 and ε_2 are given by $\mu_o^2/(68.0\ h^2c^2)$ and $\mu_o^2/158.5\ h^2c^2)$ $cm^{-1}gauss^{-2}$.

of column c). The six EPR lines of atomic oxygen arise from magnetic dipole transitions between ^3P magnetic sublevels according to the selection rules

$$\Delta M_J = \pm 1 \ , \ \Delta J = 0 \ .$$

The quadratic Zeeman effect (1) predicts the resonant magnetic fields H_a through H_f as

$$h\nu = g_1\beta H_a + C_1 H_a^2 = g_1\beta H_b - C_1 H_b^2 \qquad (3\text{-}1)$$

$$h\nu = g_2\beta H_c + C_2 H_c^2 = g_2\beta H_f - C_2 H_f^2 \qquad (3\text{-}2)$$

$$h\nu = g_2\beta H_d + C_3 H_d^2 = g_2\beta H_e - C_3 H_e^2 \qquad (3\text{-}3)$$

where $g_1 = 1.500986 \pm 0.000002$ and $g_2 = 1.500921 \pm 0.000002$ (32), β is the Bohr magneton, and C_1, C_2, C_3 are constants which depend upon the spacing between the ^3P multiplets. The predicted magnetic fields at which each of the lines occur is shown in Figure 2 with each line labeled as shown in Figure 1. Transitions between the magnetic sublevels of the ^1D state are possible, however the population of these levels is so small at reasonable temperatures compared to ^3P states that observation of them is prohibited.

In order to observe an EPR line of a magnetic dipole transition, one detects the change in the Q of a microwave cavity containing, for example, a sample of a paramagnetic gas when the gas absorbs energy from the microwave magnetic field perpendicular to the static

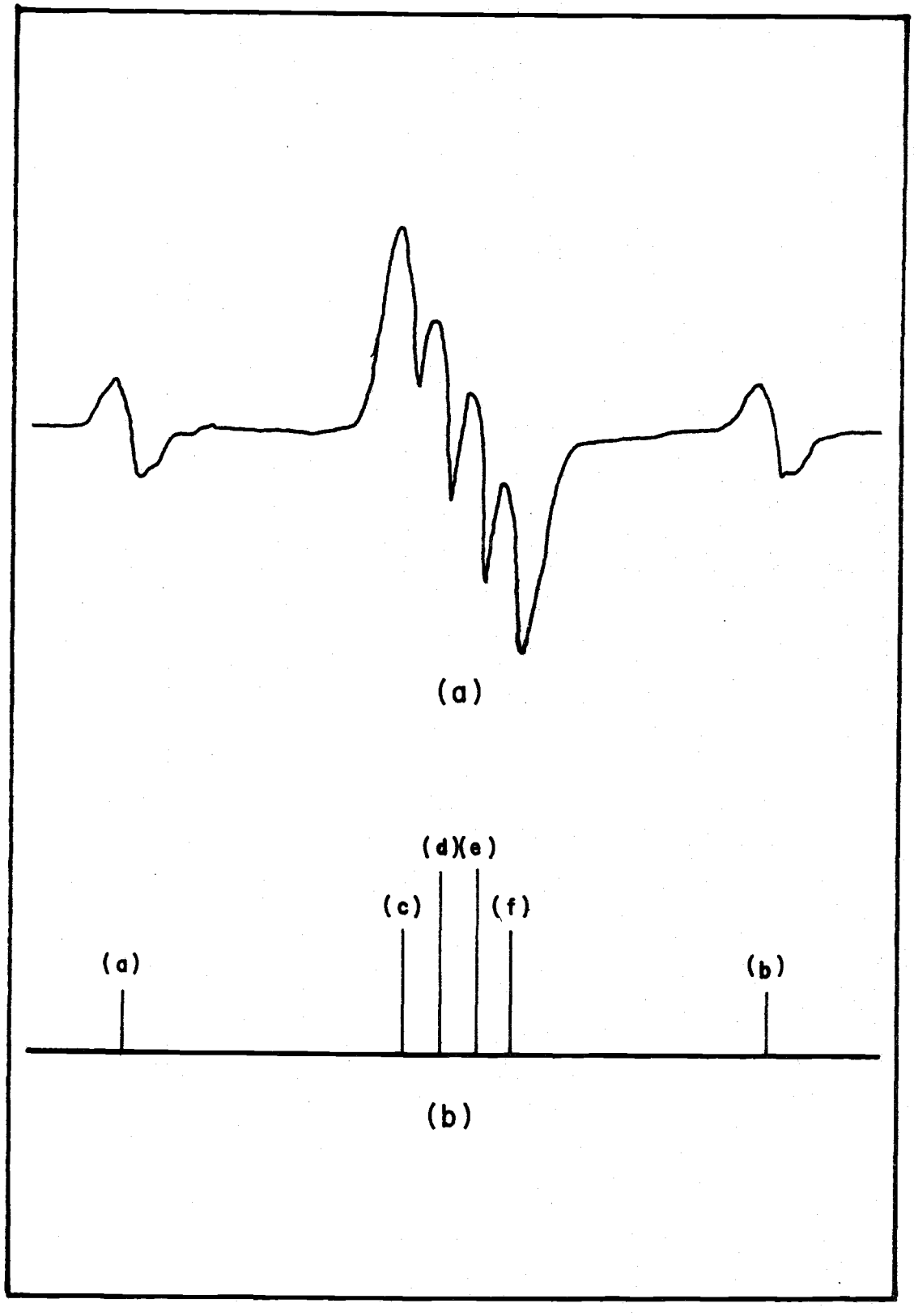

Figure 2. (a) EPR spectrum of atomic oxygen, and (b) intensity distribution of the atomic oxygen spectrum.

field H_o. The quantity which relates the absorption of energy of the gas in the cavity to the properties of the sample is just the magnetic moment per unit volume, $\vec{M}$. If a sample is placed in a magnetic field $\vec{H}$, then $\vec{M}$ is related to $\vec{H}$ by the magnetic susceptability, χ, by

$$\vec{M} = \chi \vec{H} .$$

If $\vec{H} = H_o \hat{k} + H_1 [\cos(\omega t)\hat{i} + \sin(\omega t)\hat{j}]$, i.e., a steady field H_o in the z direction and a time dependent field in the plane perpendicular to H_o, and if χ is taken to be the complex quantity

$$\chi = \chi' - i\chi'' ,$$

the power absorbed per unit volume per cycle is given (34, p. 29) by

$$P = 2 H_1^2 \omega\chi'' .$$

Since the cavity Q is inversely proportional to the power lost per cycle, the quantity which is measured by the EPR spectrometer is P, which depends upon χ'', the imaginary part of the complex magnetic susceptibility.

Van Vleck and Weisskopf (42) have derived an expression for pressure broadened microwave transitions JM, J'M'

$$\chi''_{JM,J'M'} = \frac{N}{Z}\left(\frac{\omega}{kT}\right)\exp(-E_{JM}/kT)\left|(\mu_r)_{JM,J'M'}\right|^2 f'(\omega - \omega_o) \qquad (3\text{-}5)$$

where

N is the concentration of absorbing atoms,

ω is the angular frequency of the microwaves,

E_{JM} is the energy of the JM state

$\left|(\mu_r)_{JM, J'M'}\right|^2 = g^2\beta^2 \frac{f^+}{2}(J - M)(J + M + 1)$ is the absolute square of the component of the transition matrix element in the direction of the r.f. field with f^+ the filling factor depending upon the geometry of the cavity and the sample distribution in it.

Z is the partition function,

k is the Boltzman constant,

T is the absolute temperature, and

$f'(\omega - \omega_o)$ is the Lorentzian line shape function.

The Lorentzian line shape function describes a pressure broadened line which occurs at ω_o and is given by (44)

$$f'(\omega - \omega_o) = \frac{\pi^{-1} t_2}{1 + t_2(\omega - \omega_o)^2} \qquad (3\text{-}6)$$

which is normalized so that

$$\int_{-\infty}^{\infty} f'(\omega - \omega_o)\, d\omega = 1 .$$

The quantity t_2, called the "spin-spin" relaxation time, is the reciprocal of the half-width at half-height of the Lorentzian shape function.

Since EPR experiments are in fact performed with a constant ω and a variable H, the line shape function must be changed to $f(H - H_o)$ by introducing a quantity g_{eff} (26). The term H_o is related to ω_o, the frequency corresponding to the center of the line, by $H_o = \hbar\omega_o/g\beta$. In order to make the transformation, one expands ω in a Taylor

Series about the resonance ω_o and keeps only the first two terms as an approximation to the field dependence of g at the resonance. This expansion is then compared to the resonance condition $\hbar\omega = g\beta H$ as

$$\hbar\, d\omega = g\beta\, dH \text{ and } \omega = \omega_o + \frac{\partial\omega}{\partial H} dH$$

so that $g_{eff} \equiv \frac{\hbar}{\beta}\frac{\partial\omega}{\partial H} \doteq \frac{\hbar}{\beta}\frac{(\omega - \omega_o)}{(H - H_o)}$. Thus, we may write

$$f'(\omega - \omega_o) = \frac{\hbar}{g_{eff}\,\beta} f(H - H_o) \tag{3-7}$$

where

$$f(H - H_o) = \frac{t_2\, g_{eff}/\hbar}{1 + t_2^2 \frac{g_{eff}}{\hbar^2} \beta^2 (H - H_o)^2}, \tag{3-8}$$

which then satisfies the normalization condition

$$\int_{-\infty}^{\infty} f(H - H_o)\, dH = 1 . \tag{3-9}$$

The quantity g_{eff} is just the Landé g factor for simple atomic transitions. For those transitions which split in a more complicated fashion or as a higher order function of H, the g factor in the vicinity of the transition of H_o may be approximated by g_{eff} and the resonance condition is then just $h\nu = g_{eff}\beta H$; the splitting of the states of O_2 is an example of this.

While the quadratic Zeeman effect is responsible for the observation of the six-line spectrum of atomic oxygen under conditions

of high resolution, these lines are not resolved for the conditions of this experiment. Thus, the expression for χ'' must be summed over all unresolved transitions

$$\chi'' = N \frac{(\omega_o \hbar)}{g_{at} \beta kT} \frac{1}{Z} \sum_{JM} \exp(-E_{JM}/kT) \left| (\mu_r)_{JM, J'M'} \right|^2 f(H-H_o) \tag{3-10}$$

where g_{eff} has been replaced by g_{at} and is taken out of the sum as being approximately equal for both J values. The shape factor $f(H-H_o)$ is also assumed to be independent of the summation which is approximately correct since 80% of the absorption (26) arises from nearly coincident transitions.

Electron Paramagnetic Resonance of Atomic Oxygen

Krongelb and Strandberg (26) have related the concentration of atomic oxygen to the integrated intensity of the EPR spectrum as

$$\int_{-\infty}^{\infty} \chi'' \, dH = N \left(\frac{\omega_o \hbar}{g_{at} \beta kT} \right) \frac{1}{Z} \sum_{JM} \exp(-E_{JM}/kT) \left| (\mu_r)_{JM, J'M'} \right|^2 , \tag{3-11}$$

which is independent of the shape function $f(H-H_o)$ because of Equation (3-9) and may be evaluated further. Since only the $^3P_1$ and $^3P_2$ terms contribute to the absorption, we have from (44),

$$g = 1.5 ,$$

$$Z = 5 + 3 \exp(-158.5 \, hc/kT) + \exp(-226.5 \, hc/kT) = 6.738 ,$$

$$\sum_{JM} \exp(-E_{JM}/kT)(J - M)(J + M + 1) = 21.87$$

where E_{2M} is taken as zero. Thus we have for the six line composite spectrum of atomic oxygen

$$N_O = 0.206 \left(\frac{2\,kT}{h\nu_o\, f^+ \beta}\right) \int_{-\infty}^{\infty} \chi_0'' \, dH \qquad (3\text{-}12)$$

which depends only upon known or measurable quantities, with the exception of f^+, the filling factor.

Electron Paramagnetic Resonance of Molecular Oxygen

An energy level diagram of molecular oxygen is shown in Figure 3 which shows the ground state as $X\ ^3\Sigma_g^-$. At approximately one ev above the ground level is the $a\ ^1\Delta_g$ and at 1.6 ev is the $b\ ^1\Sigma_g$ state. These last two states are metastable; the $^1\Sigma_g$ would have to violate $\Delta S = 0$ to radiate to the ground state and $^1\Delta_g$ would have to violate not only $\Delta S = 0$, but also $\Delta\Lambda = 0, \pm 1$ (18, p. 278). Both the $^3\Sigma_g^-$ and the $^1\Delta_g$ may be observed by EPR since each has a magnetic moment. It is the spectrum of $O_2(^3\Sigma_g^-)$ state which we shall deal with first.

The spectrum of $O_2(^3\Sigma_g^-)$ has a very complicated structure as is shown in Figures 4, 5, 6, which was taken in the presence of a microwave discharge and therefore also shows the atomic oxygen and $O_2(^1\Delta_g)$ spectrum as indicated. The complexity of the molecular

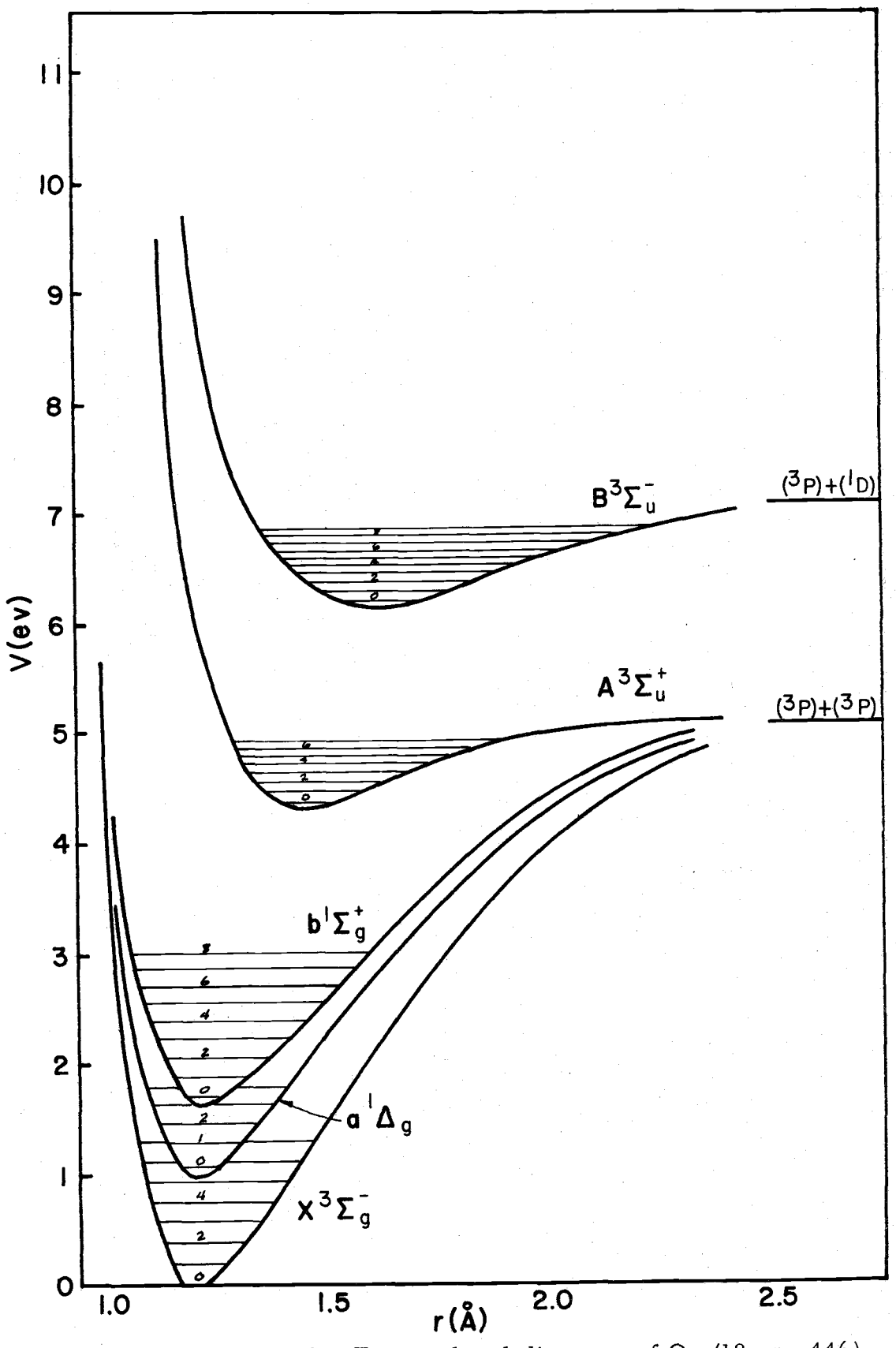

Figure 3. Energy level diagram of O_2 (18, p. 446).

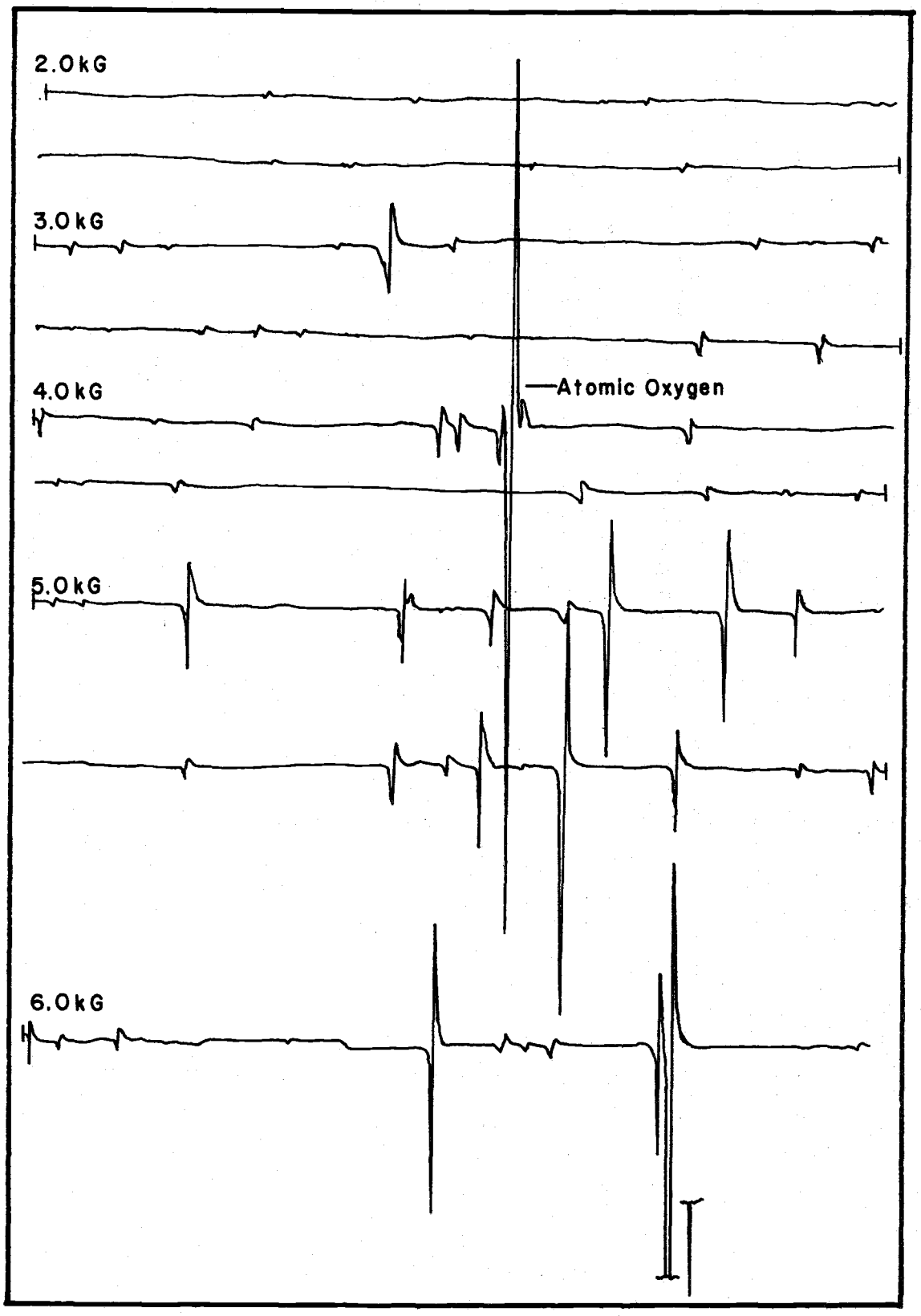

Figure 4. EPR spectrum of molecular oxygen. Part I.

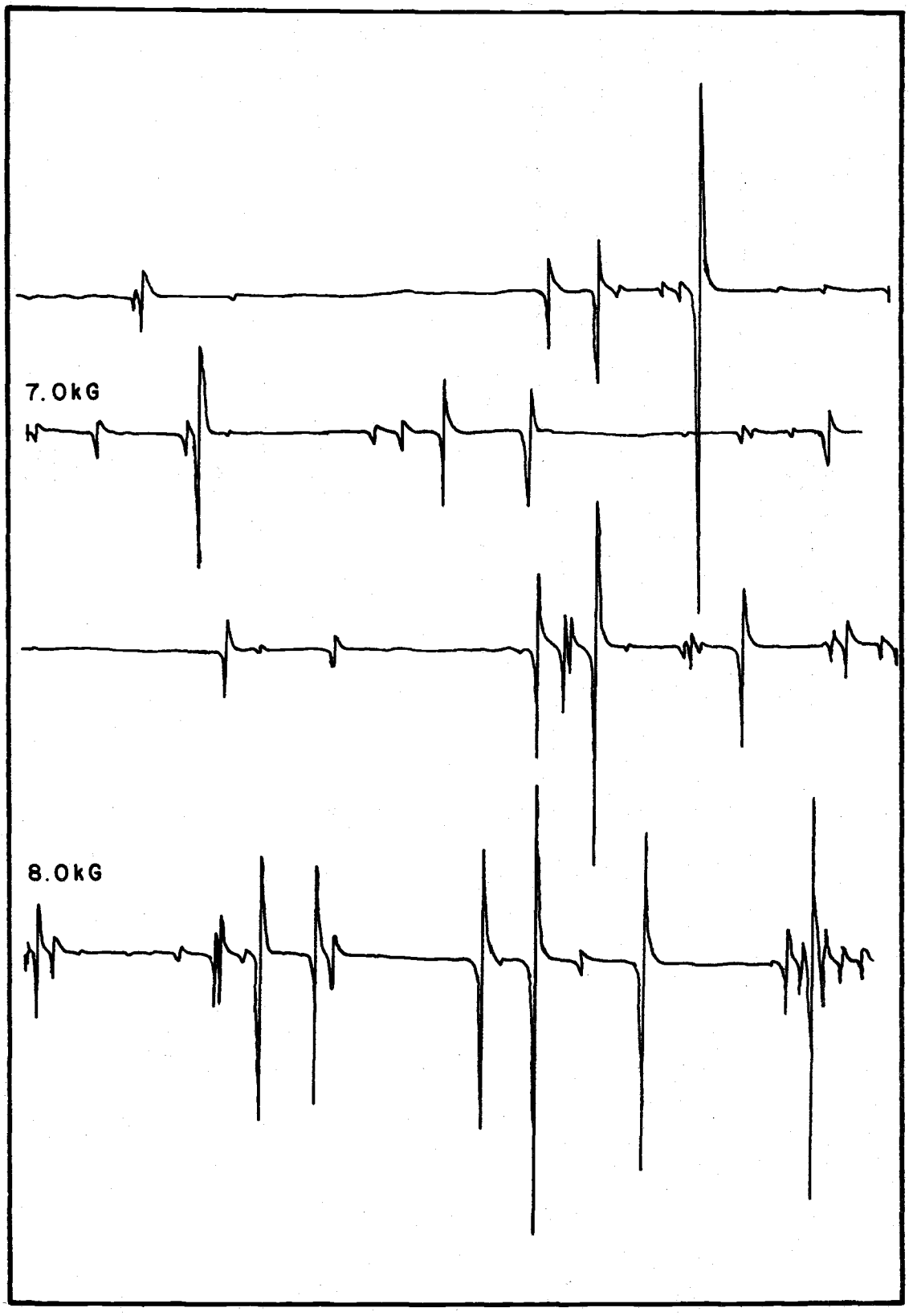

Figure 5. EPR spectrum of molecular oxygen. Part II.

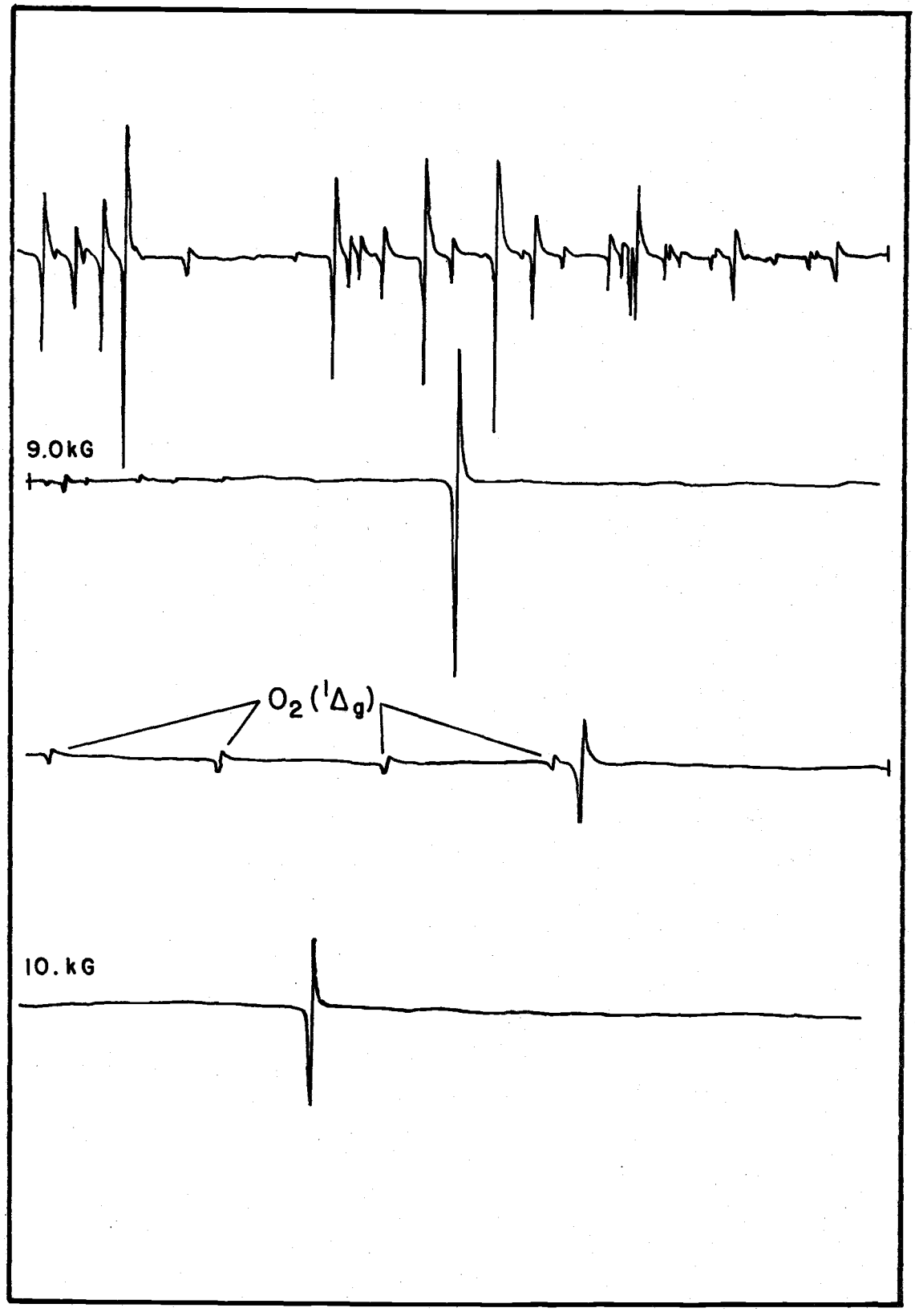

Figure 6. EPR spectrum of molecular oxygen. Part III.

oxygen spectrum arises from the coupling of the electronic and rotational angular momenta (41). The molecular absorption can be calculated using the data from Tinkham and Strandberg (41) and Equation (3-11) applied to molecular oxygen (26, 44). Thus, since each absorption is from a single line, Equation (3-11) becomes

$$\int_{-\infty}^{\infty} \chi'' \, dH = N\left(\frac{\omega_o \hbar}{g_{eff}\beta kT}\right) \frac{1}{Z} \exp(-E_{JM}/kT) \left| (\mu_r)_{JM, J'M'} \right|^2 \quad (3\text{-}13)$$

which may be evaluated for the K = 5, J = 4 → 6, and M = 1 → 2 transition which Krongelb and Strandberg (26) used. Upon evaluating the following quantities

$$\left| (\mu_r)_{JM, J'M'} \right|^2 = g^2 \beta^2 \frac{(f^+)}{2} \{4 \left| \langle JM | S_x | J'M' \rangle \right|^2 \} ,$$

$$g_{eff} = \frac{\hbar}{\beta} \frac{\partial \omega}{\partial H} \Bigg|_{H = H_o}$$

$$g = 2 ,$$

$$Z \simeq \frac{3\,kT}{2\,Bh} ,$$

B = 43, 100 MHz, the rotational temperature (43, 100 MHz is equivalent to k 2.1° K),

and from Tinkham and Strandberg (41, p. 958)

$$4 \left| \langle JM | S_x | J'M' \rangle \right|^2 \exp(-E_{JM}/kT) = .37 ,$$

$$g_{eff} = 1.313 ,$$

we have

$$\int_{-\infty}^{\infty} \chi'' \, dH = N_{O_2} \frac{\nu_o h\beta f^+}{2\,kT} \times 0.521$$

or finally

$$N_{O_2} = 1.92\left(\frac{2\,kT}{\nu_o h\beta f^+}\right)\int_{-\infty}^{\infty} \chi'' \, dH \qquad (3\text{-}14)$$

The work of Tinkham and Strandberg (41) and Krongelb and Strandberg (26) permits absolute concentration measurements, since the ratio of Equation (3-12) to Equation (3-14) yields

$$N_O = N_{O_2} (0.107) \frac{\int_{-\infty}^{\infty} \chi''_O \, dH}{\int_{-\infty}^{\infty} \chi''_{O_2} \, dH}, \qquad (3\text{-}15)$$

and since N_{O_2} is known from the pressure, one may calculate N_O.

It will be of interest to estimate the ratio of the concentration of $O_2(^1\Delta_g)$ to that of atomic oxygen. The EPR spectrum of $O_2(^1\Delta_g)$ state was first observed by Falick, Mahan and Myers (9) in oxygen passed through a microwave discharge in which they measured the ratio of the concentration of $O_2(^1\Delta_g)$ to $O(^3P)$ to be approximately 0.5. To make this determination, one must evaluate Equation (3-13) for $O_2(^1\Delta_g)$. The spectrum that was observed results from the ΔM_J = 1 transition for the J = 2 total angular momentum state which interacts with the J = 3 state to split the transitions into a nearly symmetric quartet (9). More recently, Miller (30) has observed not only the J = 2, but also the J = 3 spectra.

If we assume that the $O_2(^1\Delta_g)$ molecule is describable by Hund's case a), i.e., the orbital angular momentum of the electrons couples strongly to the internuclear axis and only weakly with the rotational angular momentum, then we may write the energy of the interaction of the magnetic field with the magnetic moment associated with the angular momentum as

$$E = g_J \beta H M_J + \text{higher order terms}$$

where

$$g_J = \frac{\Lambda^2}{J(J+1)} \; ;$$

Λ is the component of the orbital angular momentum of the electrons along the internuclear axis and J is the total angular momentum. For the $\Lambda = J = 2$, $\Delta M_J = +1$, and $\Delta J = 0$ transition, the matrix element (26, 10) becomes

$$|\langle JM_J | \mu_r | JM_{J+1} \rangle|^2 = \tfrac{1}{2} g_J^2 \beta^2 f^+ (J - M)(J + M + 1).$$

The partition function is similar to that of $O_2(^3\Sigma_g^-)$ except that the rotational constant is 43, 401 MHz (30) which gives $Z_{1_\Delta} = 210$. For the $M_J = 0$ to $M_J = +1$ transition, $E_{JM} = 0$ and

$$\exp(-E_{JM}/kT) \; |\langle J0 \, | \mu_r | \, J1 \rangle|^2 = 3\beta^2 g_J^2 f^+ .$$

Thus

$$\int_{-\infty}^{\infty} \chi''_{1_\Delta} \, dH = N_{1_\Delta} \frac{\omega_o \hbar}{g_{eff} \beta kT} \frac{3}{210} \beta^2 g_J^2 f^+ ,$$

where

$$g_{eff} = g_J = 2/3 ,$$

and the ratio of $N(^1\Delta_g)$ to $N(^3P)$ is given by

$$\frac{N(^1\Delta)}{N(^3P)} = 234 \frac{\int \chi''_{^1\Delta} \, dH}{\int \chi''_{O} \, dH} .$$

We are now able to calculate the ratio of the concentrations of $O_2(^1\Delta_g)$ to $O(^3P)$ by evaluating the two integrals, which may be done by numerically measuring the area under the EPR absorption line for each. Alternatively, because the task of numerical integration is tedious, and since we will be satisfied with an approximate concentration ratio, we will evaluate the integrals in a different manner.

Each integral is proportional to the maximum signal height of its EPR spectrum. The constant of proportionality in each case depends not only upon instrumental parameters, but also upon the line shape function which reflects the physical properties of the species whose spectrum is being observed. By taking the line shape functions approximately equal and using the same instrumental parameters, the ratio of the integrals is approximately the ratio of the maximum signal heights. Thus a measurement of the signal height of $O(^3P)$ to be 400 times that of $O_2(^1\Delta_g)$ yields an $O_2(^1\Delta_g)$ molecular concentration which is nearly half as large as that of $O(^3P)$ atoms.

CONCENTRATION MEASUREMENTS

We shall now discuss the details of using EPR techniques to make both relative and absolute concentration measurements of gases. The simplest of the methods is the relative assessment.

Relative Concentration Measurements

In this work nearly all quantitative results will be determined from relative measurements of the concentrations of atomic oxygen. If one looks at Equation (3-12) which has been evaluated for the composite six-line spectrum, one sees that the only unknown quantity is f^+, the cavity filling factor. If we evaluate $\int \chi'' \, dH$ for two different O-atom concentrations, then the ratio of these concentrations is given by

$$\frac{N_{O1}}{N_{O2}} = \frac{\left(\int \chi'' \, dH\right)_1}{\left(\int \chi'' \, dH\right)_2}$$

In order to make this evaluation, one must examine $\int \chi'' \, dH$. The integral is not the output signal of the EPR spectrometer, but some quantity related to it. The spectrometer makes use of field modulation and phase sensitive detection which produces an output proportional to the first derivative of χ'' with respect to the magnetic field. It is necessary then to know how this signal is related to χ''.

If one defines for a single line the n^{th} moment of the absorption curve as

$$M''_n \equiv \int_{-\infty}^{\infty} H^n \chi''(H)\, dH = -(n+1)^{-1} \int_{-\infty}^{\infty} H^{n+1} \frac{\partial \chi''}{\partial H}\, dH$$

then the zeroth moment is just

$$M''_0 = \int_{-\infty}^{\infty} \chi''(H)\, dH = -\int_{-\infty}^{\infty} H \frac{\partial \chi''}{\partial H}\, dH$$

which is proportional to the concentration of any particular absorbing species. Similarly, the n^{th} moment of the output signal, S(H), of the EPR spectrometer may be defined as

$$M''_n \equiv -(n+1)^{-1} \int_{-\infty}^{\infty} H^{n+1} S(H)\, dH .$$

Halbach (16) has shown that the zeroth moments of the absorption curve and the spectrometer signal as defined above are related as

$$M''_0 = \frac{\beta}{n} H_1 M''_0 ,$$

which implies that calculations from the EPR signal do indeed give the correct result if composite lines are sufficiently modulation broadened to be a single approximate Lorentzian line and if the modulation field is taken into account. Thus, relative concentration measurements may be made by evaluating the integrals in Equation (4-1), a very tedious task. Do we even have to do this? The integrals in Equation (4-1) are finite, so that, intuitively, one should be able to write

$$\int \chi'' \, dH \sim h$$

where h is a signal height. That this is the case has been shown experimentally (26, 44, 43), so that relative concentration measurements may be made from the heights of the two signals, providing parameters such as microwave power are maintained constant; these heights may be taken at the maximum of the derivative signal.

The experiment to be described here will use time-dependent signals, in which the concentration of atomic oxygen will be observed from an indicial time until the concentration has dropped effectively to zero. In this case the relative concentration at a time t is given by

$$\frac{N_O(t)}{N_O(t = 0)} = \frac{h(t)}{h(t = 0)} \qquad (4\text{-}2)$$

Absolute Concentration Measurements

From the preceding discussion it seems clear how one can measure absolute concentrations. Equation (3-15) relates N_O to N_{O_2} and the ratio of two integrals which may be evaluated by numerical integration. However, the implication there is that all instrumental parameters can be held constant. Generally speaking, this will not be true, and for completeness it will be indicated how the parameters enter into the absolute measurement of the atomic oxygen concentration using O_2 as a calibration. Westenberg and de Haas (44) give

$$\frac{X_{at}}{X_{O_2}} = Q_{at}\left(\frac{M_{O_2}}{M_{at}}\right)\left(\frac{P_{cal}}{P}\right)\left(\frac{I_{at}}{I_{O_2}}\right)\left(\frac{W_{O_2}}{W_{at}}\right)^{\frac{1}{2}} \qquad (4\text{-}3)$$

where

X_{at} = the mole fraction of the atomic species,

X_{O_2} = the mole fraction of molecular oxygen,

P_{cal} = the calibration pressure,

P = the experimental pressure,

W_{O_2} = the power level for calibration,

W_{at} = the power level for the experiment,

M_{O_2} = the modulation amplitude for calibration,

M_{at} = the modulation amplitude for the experiment,

I_{at} = the integrated intensity for atomic transitions,

I_{O_2} = the integrated intensity for the calibration line, and

$$Q_{at} = \frac{0.206\, g_{at}^2\, p}{g_{eff}\, Z_{O_2}}$$

where

$$p = [4|S_x|^2_{JM, J'M'}]\ \exp(-E_{JM}/kT),$$

$$Z_{O_2} = \frac{3\,kT}{2Bh}, \text{ and}$$

$B = 43,100$ MHz.

If the atoms are mixed with O_2, then $P = P_{cal}$, $X_{at} = N_{at}/P$, and $X_{O_2} = N_{O_2}/P$ which is equivalent to Equation (3-15) taken at the same modulation amplitude and power levels. Equation (4-3) doesn't

include the possibility of different amplifier gains used for the two runs. If the gains are different, the right-hand side of Equation (4-3) must be multiplied by the quantity $\left(\frac{SL_{O_2}}{SL_{at}}\right)$.

Having laid the foundation for making concentration measurements using EPR techniques, we turn to atomic oxygen recombination.

MODEL FOR OXYGEN RECOMBINATION

The model which is chosen to describe the recombination of oxygen depends upon the relative concentrations of the atomic and molecular species present.

The Production of Oxygen Atoms by Microwave Discharge

One of the most efficient ways to produce atomic oxygen is by the use of a microwave discharge. In the discharge electrons excite, ionize, and dissociate the gas so that large concentrations of ions, atoms and, excited atoms and molecules are present.

Wall recombination is a major mechanism by which oxygen atoms combine in any sort of enclosure. The rate of this reaction is first order in [O] and is sufficiently large to make measurements of other concomitant reactions difficult unless some means is employed to reduce the recombination efficiency of the wall. There appears to be an approximate relationship between the recombination efficiency and the acidity of the surface (22); the more acidic the surface the less the probability of combination. Thus, the treatment of the surfaces with HF, HNO_3, or H_3PO_4 reduces the surface activity (22, 45).

The wall recombination efficiency γ is defined as the ratio of the number of wall recombinations per second per unit area to the

total number of collisions with the wall per second per unit area. From the kinetic theory of gases we have that the number of atoms striking any surface per unit time per unit area is given by $\frac{1}{4} n \bar{c}$ where $\bar{c}$ is the average thermal speed of the atoms and n is the concentration of the atoms. Thus the number of recombinations per unit area per unit time, N', may be expressed as

$$N' = \tfrac{1}{4} \gamma \, n \bar{c} \, . \tag{5-1}$$

For wall recombination one may write the following rate equation

$$\frac{dn}{dt} = -k_w \, n \, , \tag{5-2}$$

which says that the time rate of loss of atomic concentration, n, caused by collisions with the wall is proportional to n. Thus, from Equation (5-1) and Equation (5-2) we can express the number of recombinations per unit time at the wall as

$$\tfrac{1}{4} \gamma \, n \bar{c} \cdot \text{Area} = k_w \, n \cdot \text{Volume},$$

so that for a right circular cylindrical cavity of radius, r, and height $h = \beta r$, where β is a scaling factor, we have

$$\gamma = \frac{2 k_w r}{\bar{c}} \quad \frac{\beta}{1 + \beta} \quad . \tag{5-3}$$

There are two heterogeneous volume reactions which consume atomic oxygen, both first order in [O]. The first, Reaction (2-3) from Table II, which also depends upon $[O_2]$ and [M], is a production mechanism for ozone. The third body, M, is most likely to be O_2 in

the conditions of this experiment, since, except in the discharge region, nearly all the gas is O_2. The rate constant at 300° K for this reaction has been measured by Kaufman (24) to be 6.5×10^{-34} $cc^2/molecule^2$ sec. The other heterogeneous reaction, Reaction (2-4) in Table II, consumes O-atoms and O_3 molecules, and, together with the previous reaction, predicts $[O_3]$ will reach its steady state value. The rate constant for this reaction was measured by Benson and Axworthy (5) to be 4.2×10^{-15} cc/molecule sec.

There is a homogeneous three-body volume recombination reaction which removes oxygen atoms. This is Reaction (2-2) in Table II with an experimentally determined (39) rate constant of 4.5×10^{-33} $cc^2/molecule^2$ sec, which is an order of magnitude greater than that for Reaction (2-3). However, since $[O] \doteq 10^{-2}[O_2]$ initially and since Reaction (2-2) is a second order reaction, the heterogeneous reaction dominates. Therefore, the second order reaction will be neglected in the model we construct.

In discharged oxygen there is much evidence (9, 33, 13, 3) for the existence of O_2 in the $a^1\Delta_g$ metastable state in concentrations from 0.2 (9) to 0.5 (33) times [O] and the existence of O_2 in the $b^1\Sigma_g^+$ metastable state (33, 13, 3). The presence of these excited species leads to the possibility that they react with O_3 (23, 3) to produce atomic oxygen according to Reaction (2-5) of Table II. While Kaufman and Kelso (23) feel that the concentration of $O_2(^1\Sigma_g^+)$ is too small to be an

important factor in O-atom production, the reaction of $O_2(^1\Delta_g)$ is a mechanism which must be taken into account, otherwise its neglect leads to a rate constant for the Reaction (2-3) which is too small.

The $O_2(^1\Delta_g)$ state, as has been indicated, is metastable, having an extremely long radiative life, approximately 60 min. (12). Attempts, which were successful in quenching the $O_2(^1\Sigma_g)$ state by adding water vapor, failed with $O_2(^1\Delta_g)$. However, small amounts of ethylene injected downstream after oxygen atoms were removed by reacting them with NO were successful in quenching this long-lived species (9).

Thus, one must use the following reactions if one is to explain atomic recombination data taken using a discharge in oxygen.

$$O + O\cdot S \rightarrow O_2 \qquad (5\text{-}4)$$

$$O + O_2 + O_2 \rightarrow O_3 + O_2 \qquad (5\text{-}5)$$

$$O + O_3 \rightarrow O_2 + O_2 \qquad (5\text{-}6)$$

$$O_2(^1\Delta_g) + O_3 \rightarrow O + O_2 + O_2 \qquad (5\text{-}7)$$

The Production of Oxygen Atoms by Pyrolysis of Ozone

The difficulty caused by the necessity of including the $O_2(^1\Delta_g)$ reaction in any model using discharged oxygen, namely that one cannot solve the rate equation, makes the production of O-atoms by

pyrolysis of ozone very attractive in spite of the danger[3] involved.

If a stream of ozone is passed through an oven at a temperature 800° C to 1200° C nearly all the ozone is dissociated (23) into O and O_2 by the reaction

$$O_3 \rightarrow O + O_2$$

having a rate constant at 900° C of 3.5×10^{-13} cc/molecule sec.

The object of using pyrolysis of ozone as a source of oxygen atoms was to eliminate any $O_2(^1\Delta_g)$ reactions. To see if this obtained, ozone was passed through an oven at approximately 1200° C and the products allowed to diffuse into the cavity of the EPR spectrometer which was able to observe the four line spectrum of $O_2(^1\Delta_g)$ when the atoms were produced by a discharge. At the highest possible sensitivity of the instrument, no $O_2(^1\Delta_g)$ spectrum was observed in the products of the pyrolyzed O_3. Therefore, experimentally, the reaction represented by Equation (5-7) could be eliminated from the recombination model.

---

[3]Concentrated ozone has a history of detonation. Benson and Axworthy (4) report eight explosions in ozone at high pressures and the experiment reported here was terminated by such a detonation at approximately 100 torr.

REACTION KINETICS

Having selected a model based upon the pyrolysis of ozone as a source of oxygen atoms, the Law of Mass Action, which states that the rate of a chemical reaction is proportional to the concentration of the reactants, leads to the differential equations which express the kinetics of this model. Let the following be defined:

$$1)\ n_1 \equiv [O]$$

$$2)\ n_2 \equiv [O_2]$$

$$3)\ n_2 \equiv [O_3]$$

The Differential Equations for the Reactions

The reactions given by Equations (5-4), (5-5), and (5-6) lead to the differential equations

$$\frac{dn_1}{dt} = -k_w n_1 - k_1 n_1 n_2^2 - k_2 n_1 n_3 , \qquad (6\text{-}1)$$

$$\frac{dn_3}{dt} = k_1 n_1 n_2^2 - k_2 n_1 n_3 , \qquad (6\text{-}2)$$

a set of two coupled equations in which essentially only n_1 and n_3 are time dependent since we shall assume that n_1 and n_3 are very much smaller than n_2, i.e., the total pressure is made up entirely by O_2.

Solution Using Steady-state Approximation

The solution to these coupled equations depends upon additional

assumptions about the conditions of the reaction. If n_3 reaches steady-state, n_{3ss}, in a time which is short compared to the mean life of the oxygen atoms, then setting $\frac{dn_3}{dt} = 0$ in Equation (6-2) leads to two solutions, either 1) n_1 is zero or 2)

$$n_{3ss} = n_2^2 k_1/k_2 , \tag{6-3}$$

a quantity which increases with the square of the pressure. The Equations (6-1) and (6-2) may be rewritten in terms of n_{3ss} as

$$\frac{dn_1}{dt} = -n_1 \{k_w + 2 k_1 n_2^2 + k_2(n_3 - n_{3ss}) \} \tag{6-4}$$

$$\frac{dn_3}{dt} = n_1 k_2(n_{3ss} - n_3) . \tag{6-5}$$

Equation (6-5) shows that if the initial value of O_3, n_{30}, is not equal to n_{3ss}, then the reaction will proceed in the direction to establish that equilibrium. Equation (6-4) predicts that the rate at which O-atoms are used up depends not only upon the square of the pressure, but also the discrepancy between n_3 and its equilibrium value.

If one assumes that n_{3ss} is reached very rapidly compared to the decay of n_1, then Equation (6-1) becomes

$$\frac{dn_1}{dt} = -k_w n_1 - 2 k_1 n_2^2 n_1 , \tag{6-6}$$

which has the solution

$$n_1 = n_{10} \exp(-\alpha t) , \tag{6-7}$$

where n_{10} is the O-atom concentration at t = 0, and

$$\alpha = k_w + 2k_1 n_2^2 . \qquad (6\text{-}8)$$

Thus, the assumption that n_3 reaches its steady state value implies that n_1 decays exponentially in time for a fixed pressure, and that a plot of α as a function of (pressure)^2 will yield a y-intercept that is k_w and a slope that is $2k_1/k^2T^2$ where k is the Boltzman constant and T is the absolute temperature.

Failure of the Steady-state Approximation

Many data were taken as described in the next chapter, using a microwave discharge as a source of atoms and with pressure as a parameter. These data were plotted on semi-log graph paper in the form n_1/n_{10} as a function of time. The data were very erratic and Figure 7 shows a sample of some of the semi-log plots. The obvious characteristic of these plots is that the decays aren't always exponential. If one examines Equation (6-4), a possible reason becomes apparent.

The condition that $\frac{dn_3}{dt} = 0$ was also satisfied by $n_1 = 0$, which dictates the possibility that if n_{30} were far enough from n_{3ss} so that enough of the atomic oxygen was used up before reaching n_{3ss}, then n_3 approaches an equilibrium value different from n_{3ss}; call it $n_{3\infty}$. $n_{3\infty}$ can have any value, but if $n_{30} > n_{3ss}$, then Equation (6-4) shows

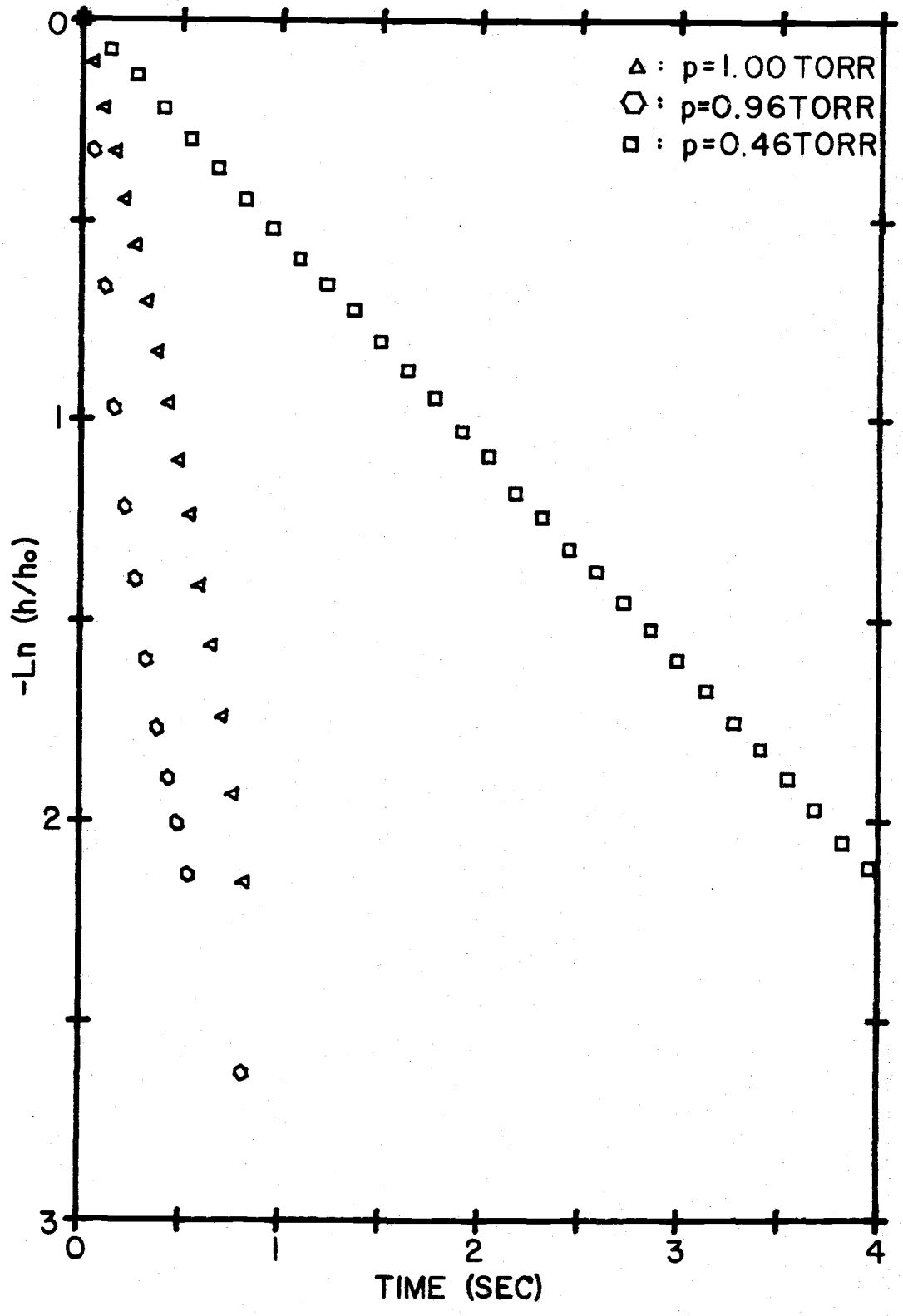

Figure 7. Sample of atomic oxygen decay curve shapes.

an initial decay which is faster than that for the pure exponential, but the decay becomes constant when n_1 reaches zero at a value whose slope is greater than α. If $n_{30} > n_{3ss}$, but n_3 reaches n_{3ss} slowly, then the same holds, except that the final slope will be equal to α. The same argument shows what can happen if $n_{30} < n_{3ss}$. The curve falls off initially slower than α, but becomes constant when n_3 reaches $n_{3\infty}$, i.e., when all the O-atoms are gone. If $n_{30} < n_{3ss}$, but reaches n_{3ss} slowly, then the final slope will be α. With all these possibilities, the question becomes whether the effects are large enough to account for data similar to those shown in Figure 7?

To see what Equations (6-1) and (6-2) would predict concerning the relationship between O and O_3, decay curves were generated by the use of a digital computer for various pressures and initial O-atom and ozone concentrations. Omitting wall effects, and using approximate rate constants, these equations may be written as

$$\frac{d(\ln Q)}{dt} = -2\,C + P \doteq -\,p^2 + P \qquad (6\text{-}9)$$

$$\frac{d(\ln P)}{dt} = -\,Q \qquad (6\text{-}10)$$

where

$$C \equiv k_1\, n_2^2 \doteq \frac{0.6\ p^2}{\text{torr}^2\ \text{sec}}$$

$$a \equiv k_2$$

$$Q \equiv n_1$$

$$P \equiv n_{3ss} - n_3 = \frac{C}{a} - n_3$$

and n_1 and n_3 are expressed in units of 10^{14}/cc. Representative curves generated in this manner are shown in Figures 8, 9, 10, 11 and 12 which indicate that only under special conditions does O_3 reach steady state very rapidly, if at all. The effect of the walls is to remove O-atoms even faster and make attainment of the ozone steady state less likely.

There is the possibility that the data shown in Figure 7, since they were taken in discharged oxygen, could be explained by the $O_2(^1\Delta_g)$ reaction with ozone. This reaction, while it can alter the steady state ozone concentration predicted above, cannot cause n_{3ss} to be realized more rapidly. Thus, one must find a way to solve Equations (6-1) and (6-2) without requiring use of the ozone steady-state approximation.

Simultaneous Solution of the Differential Equations

In order to determine α from the two differential equations (6-1) and (6-2) without making the steady state approximation, and since n_3 cannot conveniently be measured as a function of time, n_3 must be eliminated from the equations.

The solution is accomplished by solving Equation (6-2) for n_3

$$n_3 = n_{30} + n_1 - n_{10} + \alpha \int_0^t n_1 \, d\tau \qquad (6\text{-}11)$$

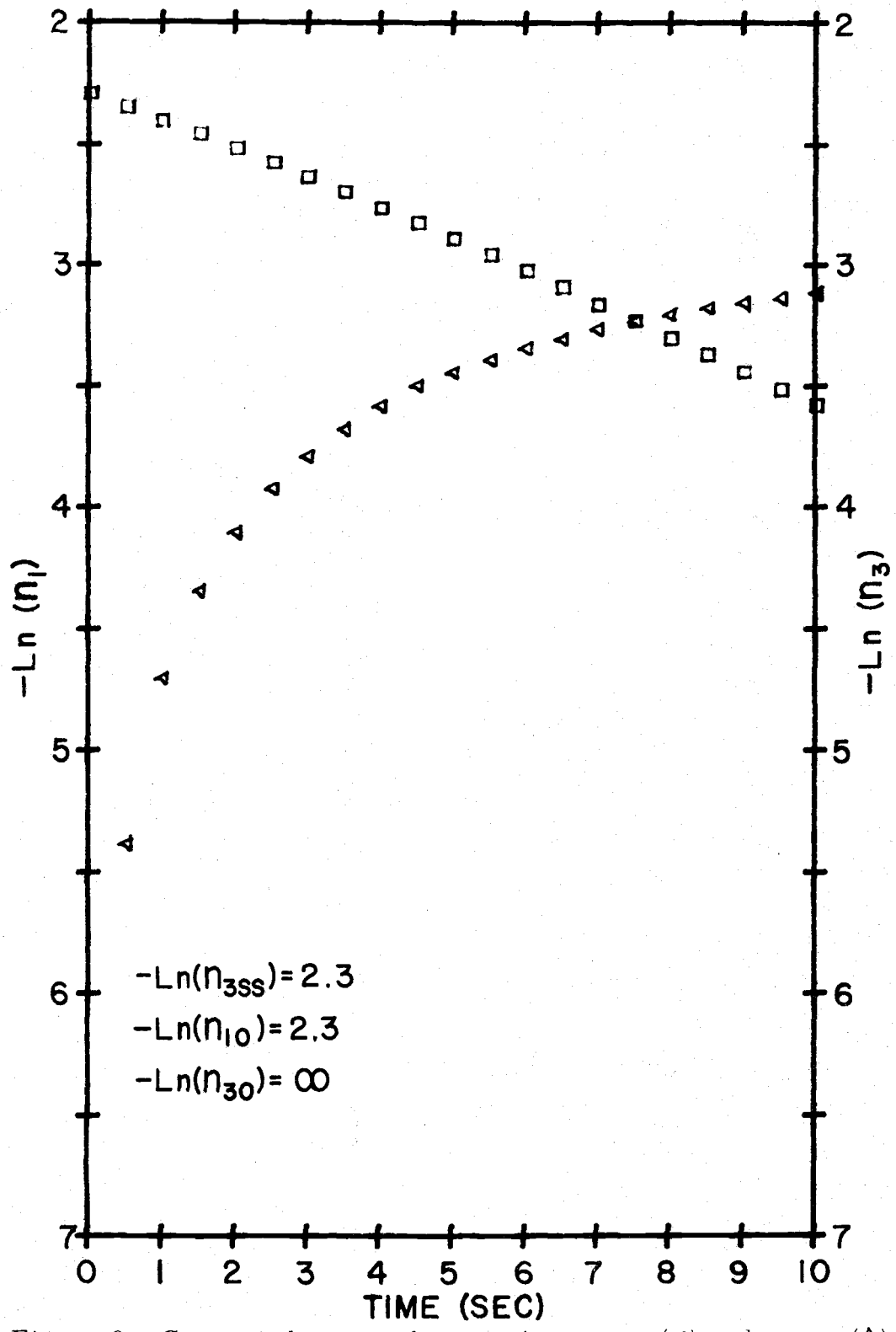

Figure 8. Generated curves for atomic oxygen (□) and ozone (△) in units of 10^{14}/cc.

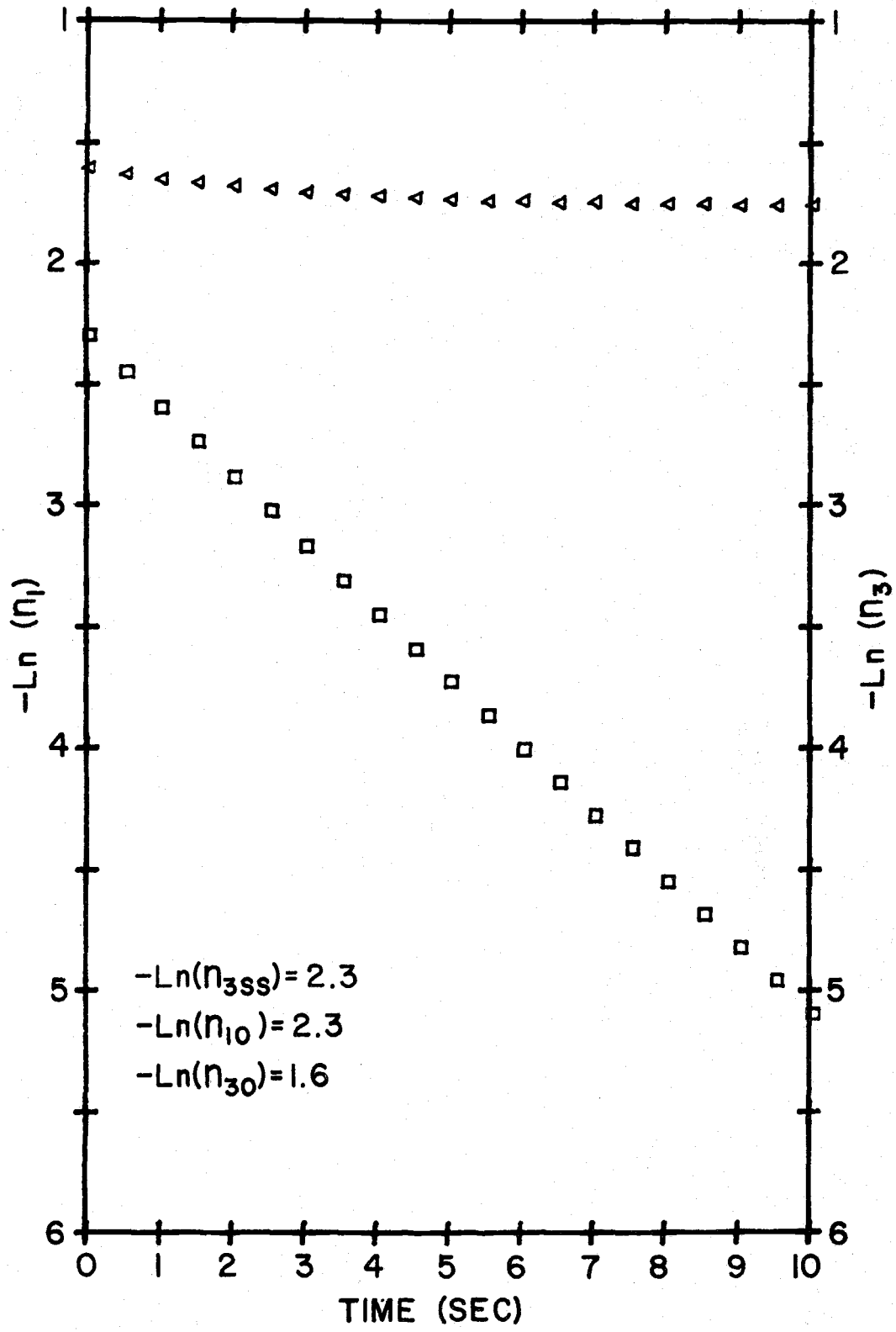

Figure 9. Generated curves for atomic oxygen (□) and ozone (△) in units of 10^{14}/cc.

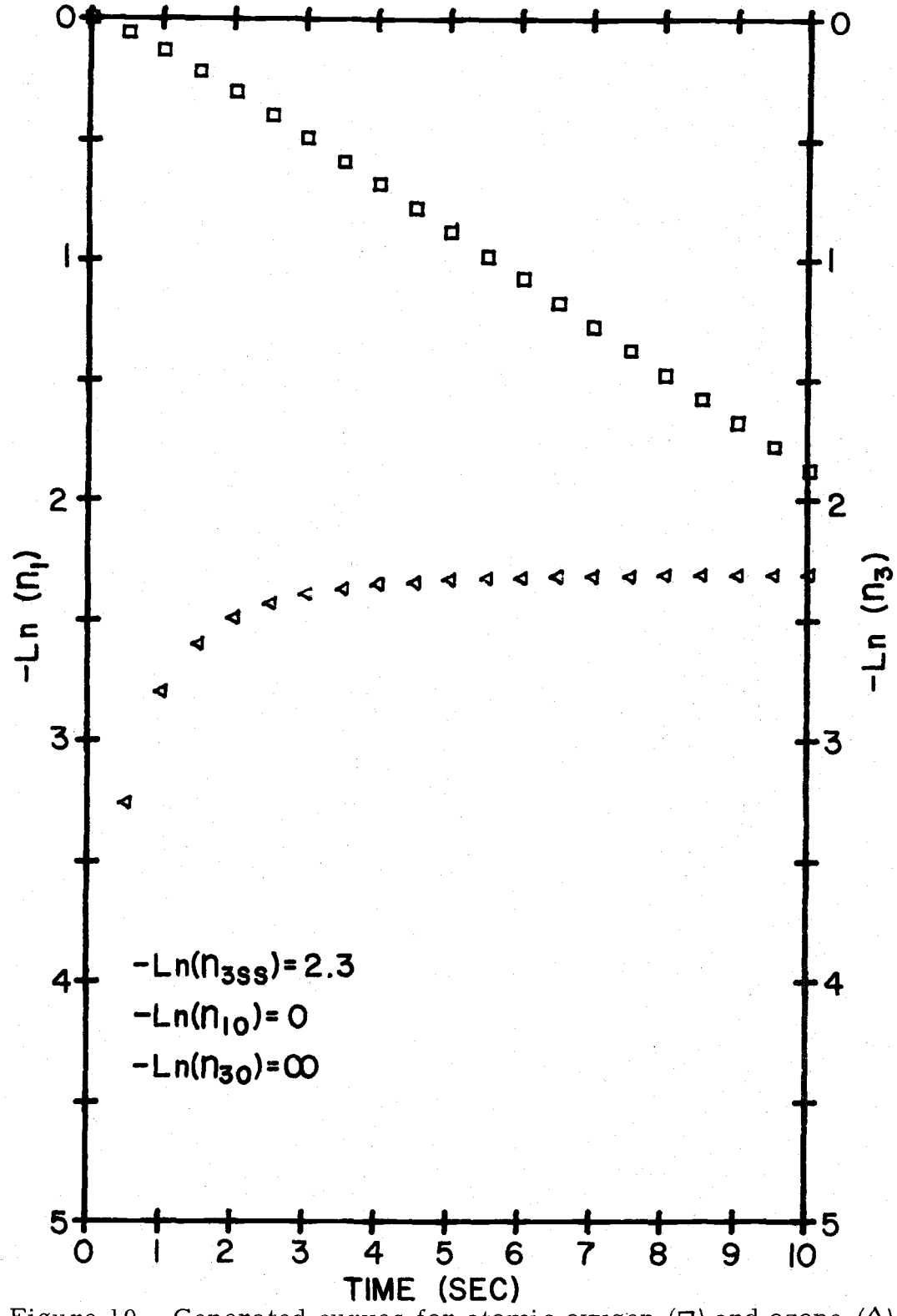

Figure 10. Generated curves for atomic oxygen (□) and ozone (△) in units of 10^{14}/cc.

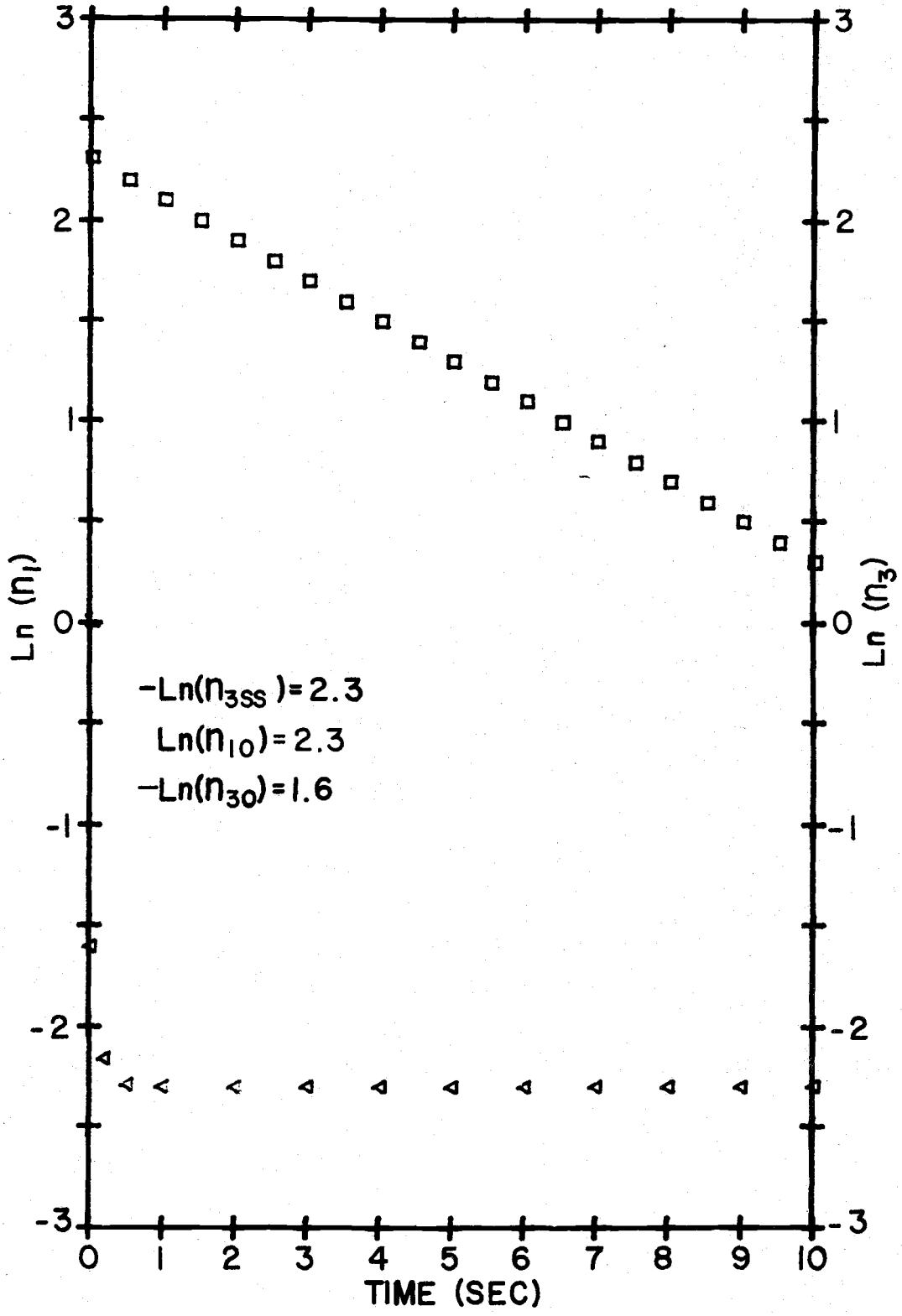

Figure 11. Generated curves for atomic oxygen (□) and ozone (△) in units of 10^{14}/cc.

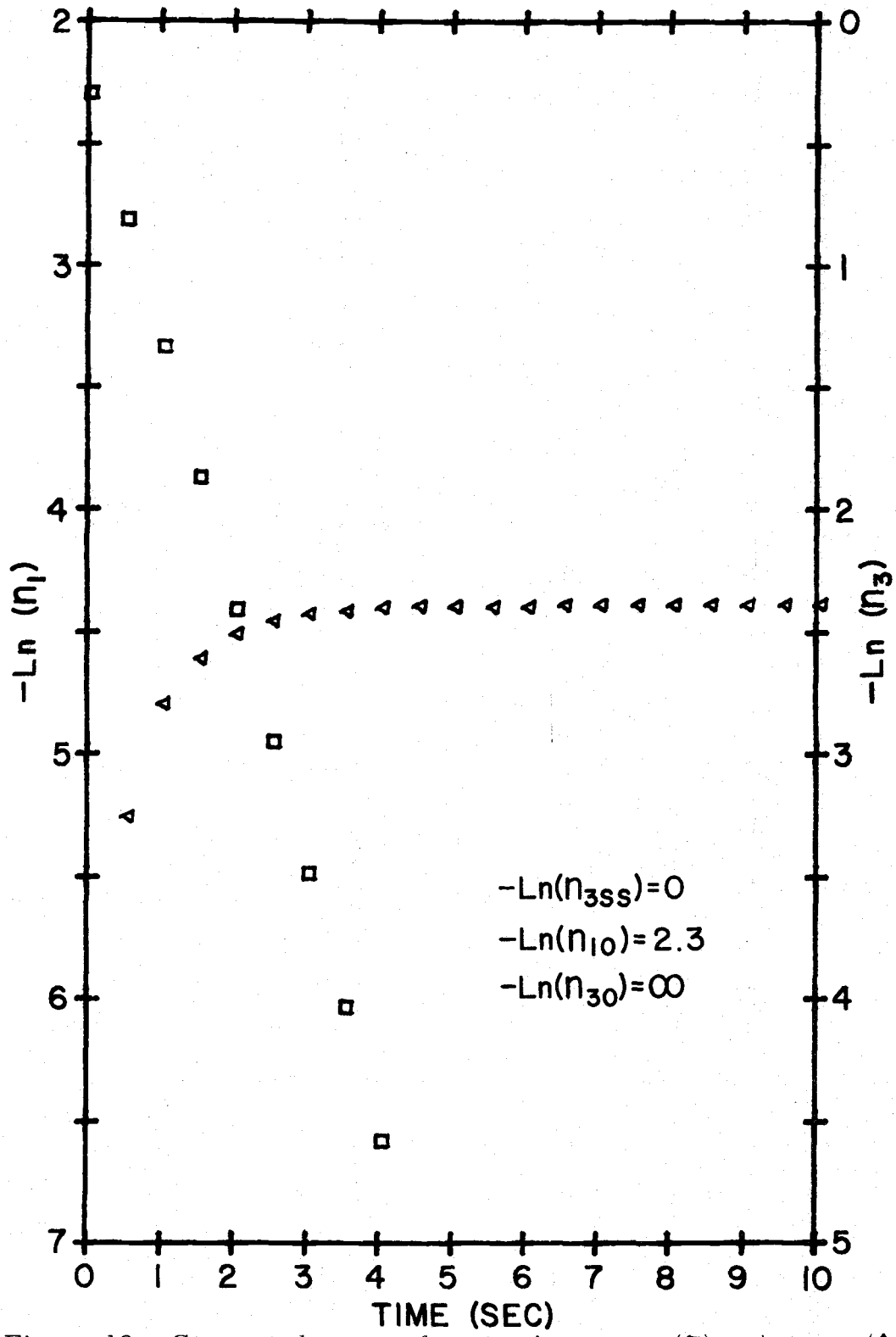

Figure 12. Generated curves for atomic oxygen (□) and ozone (△) in units of 10^{14}/cc.

and substituting this equation for n_3 into Equation (6-1) and solving for n_1

$$\mathrm{Ln}(n_1/n_{10}) - d[\mathrm{Ln}(n_1/n_{10})]/dt\,|_{t=0}\, t = -k_2\, n_{10}\int_0^t \left(\frac{n_1}{n_{10}} - 1\right) d\tau$$

$$- \alpha\, k_2\, n_{10}\int_0^t (t - \tau)\frac{n_1}{n_{10}}\, d\tau \qquad (6\text{-}12)$$

which may be written in the form

$$F(t) = - A\, H(t) - B\, G(t) \qquad (6\text{-}13)$$

where

$$F(t) \equiv \int_0^t \left(\frac{n_1}{n_{10}} - 1\right) d\tau\,,$$

$$G(t) \equiv \int_0^t (t - \tau)\frac{n_1}{n_{10}}\, d\tau\,,$$

$$H(t) \equiv \mathrm{Ln}\left(\frac{n_1}{n_{10}}\right) - \frac{d}{dt}\,[\mathrm{Ln}(n_1/n_{10})]\,\Big|_{t=0}\, t\,,$$

and

$$A \equiv (k_2\, n_{10})^{-1}$$

$$B \equiv \alpha = k_w + 2\, k_1\, n_2^2\,.$$

A FORTRAN program was written to fit, in the least squares sense, Equation (6-13) to the data for the constants A and B. The details of the fitting equations and the computer programming are listed in Appendices I and II.

THE EXPERIMENTAL APPARATUS

The relative O-atom concentration for various pressures was measured as a function of time using a Varian Model V-4501 Spectrometer which consisted of a console, a 100 KHz Field Modulation and Control Unit, a Low-High Power Microwave Bridge, a Six Inch Magnet with a 25 mm gap and Rose shimmed pole faces, and a Magnet Power Supply employing field regulation. A block diagram of the spectrometer system is shown in Figure 13.

Since atomic oxygen EPR exhibits no power saturation, high power could be used, except that if the 100 mwatt maximum klystron output wasn't attenuated at least 15 db, an apparent cyclotron resonance of electrons at g = 2 appeared in the cavity, which was completely detuned. In the high power configuration the klystron is locked to the resonant frequency of the cavity by the automatic frequency control and one is insured of observing the pure absorption mode, which gives a signal proportional to χ''.

The Cavity

The cavity employed in this experiment was constructed in this laboratory, and is similar to that of Evenson (8). It allows continuous monitoring of the decay of O-atoms upon closing the valve to the cavity. The cavity is a right circular cylinder, approximately

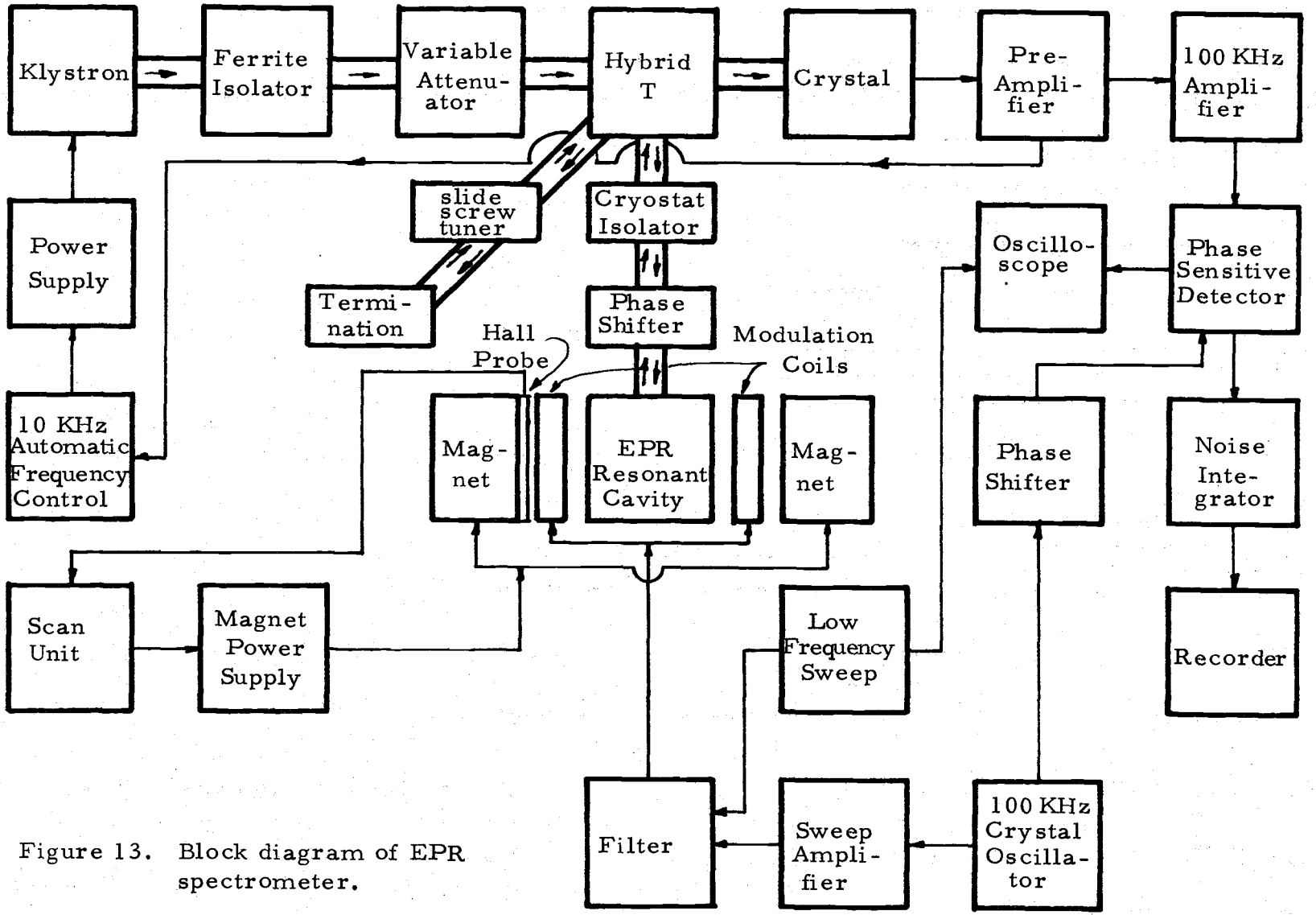

Figure 13. Block diagram of EPR spectrometer.

22 mm O. D., 25 mm long, and one mm wall thickness. It is coated on the inside with a fused 35% metaphosphoric acid-sodium metaphosphate mixture to reduce wall recombinations (35). This internal coating was accomplished by placing ten to twelve crystals of the metaphosphoric acid mixture in the cavity before silvering, heating with a hot air gun while the cavity was evacuated until the crystals melted. The liquid was then allowed to run around the inside as the cavity was tilted until the surface was entirely covered; the excess was allowed to run out the entrance stem and into a specially ground glass tube which kept the liquid from recrystallizing on the ground glass surface of the cavity valve. After a satisfactory coating had been placed on the inside, the cavity was silvered on the outside.

Evenson (8) used Brashear's process to coat his cavity with silver to a thickness of eight μm using 11 applications. The silvering of this cavity was accomplished by placing two thin coats of silver by Brashear's method and then electroplating until approximately 60 μm was deposited, as determined by calculation. This thickness represents nearly 100 skindepths at 10 GHz, but a fraction of a skindepth at 100 KHz, the magnetic field modulation frequency.

The cavity will resonate in three modes within the range of the Varian reflex klystron, the TM_{010}, TM_{011}, and TE_{111} modes. The mode used is the TM_{010}, since its magnetic field pattern is perpendicular to the axis of the cylinder, independent of the length of the

cylinder, and has the largest average magnetic intensity over the volume of the cavity. The Q is of the order of 5000 without the internal coating, but somewhat less with the coating applied. Because the coating is hygroscopic and any water combines with the meta-phosphoric acid to form orthophosphoric acid, the cavity Q will deteriorate with time if any water vapor gets into the cavity.

Microwaves are coupled into the cavity through a six mm hole in the silver on the sidewall midway between the ends of the cavity. The cavity is clamped to a mount which positions it so that it is coupled to a section of wave guide and a flange. The cavity and mount are illustrated in Figure 14. The mount is machined from plexiglass, fitted with a coupling iris, and silvered on the inside similar to that on the cavity. Fitted coaxially to the cavity when it is in the mount, and plane with it, are two Nylon coil forms. Each of these coils contains 200 turns of #40 AWG enameled magnet wire. They constitute a Helmholtz pair which gives a fairly uniform modulation field over the volume of the cavity.

The cavity is closed off from the source of oxygen atoms by a ground glass valve actuated by air pressure. The valve mechanism itself is just a 12 mm glass plate ground flat and smooth with cerium oxide grinding compound and mated against a similarly ground seat at the entrance to the cavity. To insure a tight seal, concentrated orthophosphoric acid, which remains effective for several weeks, is

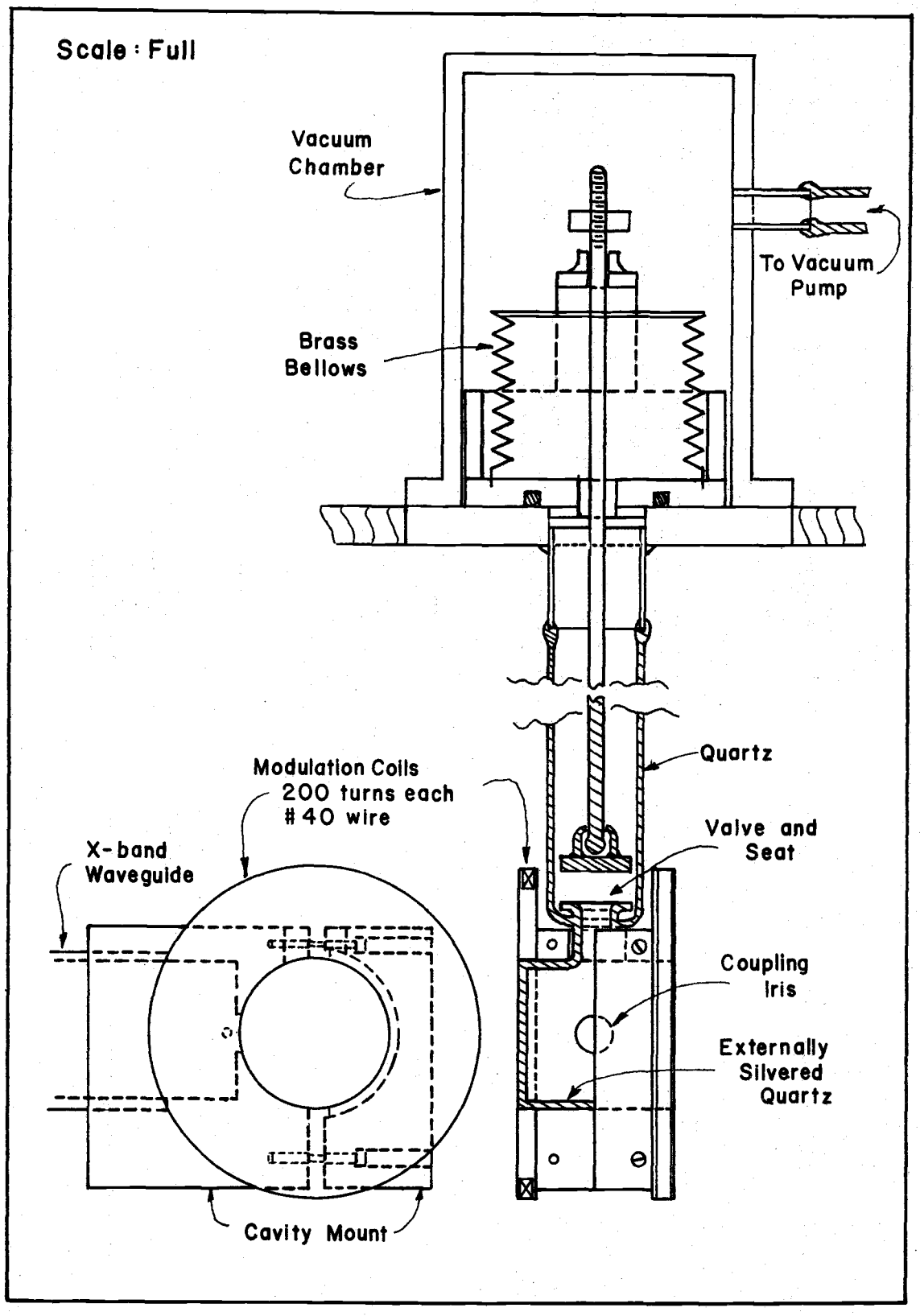

Figure 14. Quartz EPR cavity, valve, and actuator.

spread over the ground surfaces. The opening and closing of the valve is accomplished by a 30 cm rod attached to a stainless steel plate which closes one end of a brass bellows (see Figure 14). Thus, the bellows forms one end of an arm connected to the gas handling system, which is at low pressure during the experiment. The outside of the bellows is enclosed in an air-tight chamber which can be either opened to atmospheric pressure, or connected to a vacuum line. To open the valve, one merely pumps out the exterior chamber and the bellows takes on its unstressed shape. To close the valve, air is admitted rapidly, compressing the bellows. The length of travel is controlled by an adjustable stop, while the pressure of the valve makes on the seat is determined by a spring shock absorber in the connecting rod. The change in internal pressure of the system caused by the change in volume upon closing the valve was measured to be of the order of 0.2 mtorr, a negligible amount over the pressure range of the experiment.

Gas Handling System

A schematic diagram of the gas handling system is shown in Figure 15. For the part of the experiment using discharged oxygen, research grade gas was used. The gas from the tank was passed over quartz wool heated to 1200° C in an oven to crack hydrocarbons, then through an activated alumina trap to sorb hydrogen, and into a liquid

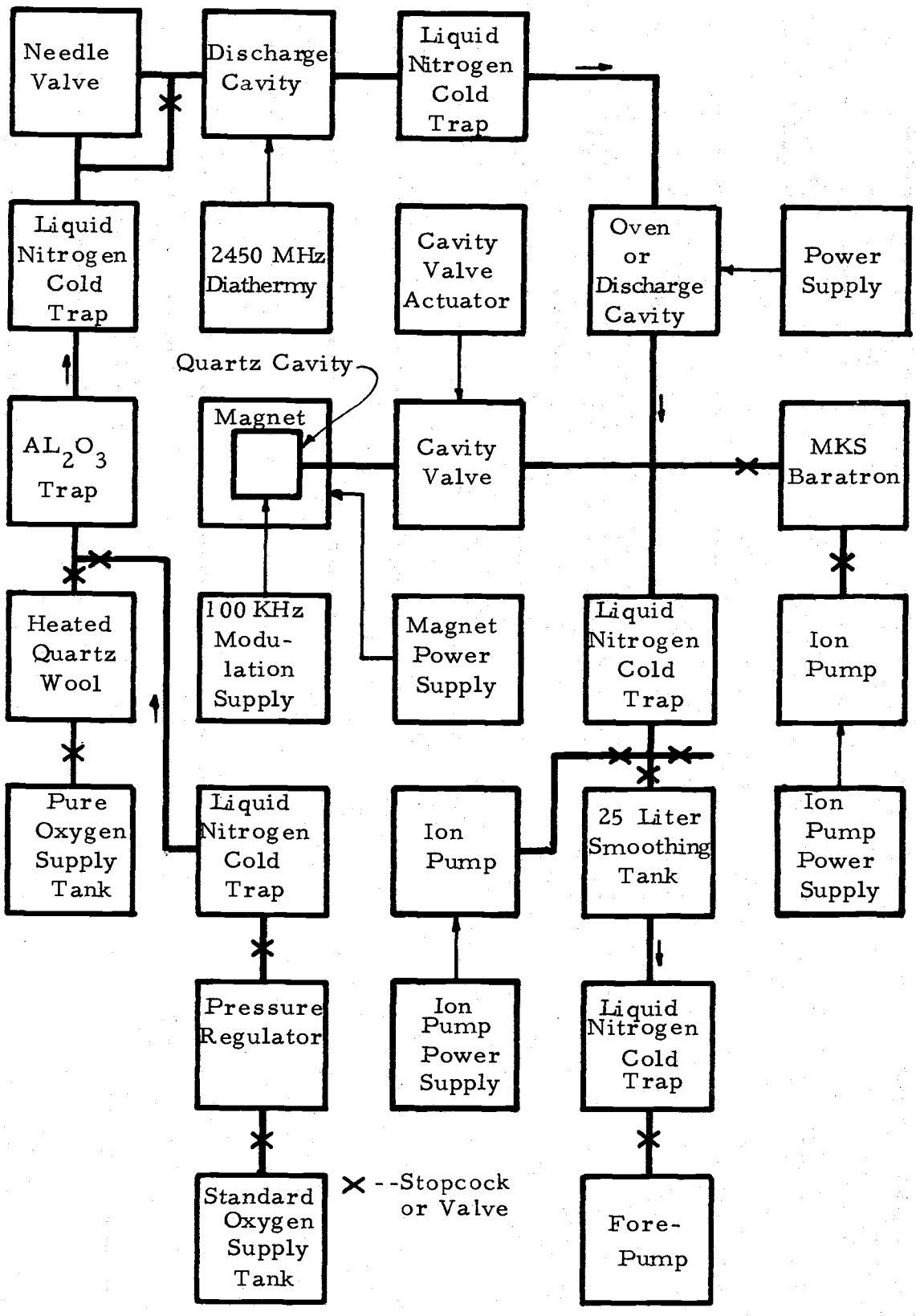

Figure 15. Gas handling system.

nitrogen trap where the O_2 was liquified. It was from this reservoir of liquid oxygen that all the gas was obtained for the experiment with discharged oxygen.

For the production of ozone, standard tank oxygen of purity 99.5% was used. This gas was passed through a liquid nitrogen trap, through an activated alumina trap to remove hydrogen and hydrocarbons, through another liquid nitrogen trap, and into a quartz tube in which a microwave discharge, the generation of which will be described in the next section, was maintained at a pressure less than 200 torr. The discharge products flowed directly into a liquid nitrogen trap in which any ozone, if its partial pressure was greater than 35 mtorr, condensed as a dark blue liquid. This procedure was found to produce about three ml of liquid in two hours.

After water is removed from the oxygen by a liquid nitrogen trap, the predominant impurity that remains is probably nitrogen. At the temperature of liquid nitrogen and the ozone collection pressure, the partial pressure of each of the probable impurities, with the exception of nitric oxide, is less than its vapor pressure. Thus, the process of the liquification doesn't retain these impurities except possibly NO since it is very efficiently produced in a discharge containing nitrogen and oxygen. If one assumes that all the oxygen impurity is nitrogen, and if in the discharge all the nitrogen is converted to NO, then the partial pressure of NO is of the order of its

vapor pressure at the temperature of liquid nitrogen, and some condensation is possible. The presence of NO even in small quantities will produce the familiar air glow spectrum from the reaction $NO + O \rightarrow NO_2 + h\nu$.

A faint air glow was visible from the discharge, indicating the possible presence of small amounts of NO. Because it takes only a minute quantity of nitric oxide to produce the air glow, it is believed that NO is not present in amounts sufficient to condense in the cold trap with the ozone. This surmise is borne out by the fact that during the pyrolysis experiment there was no evidence of an air glow downstream from the oven.

Pressures were measured by an MKS Type 77 Baratron over the pressure range from .224 to 1.10 torr with the stainless steel three torr head located approximately 125 cm from the cavity. The reference side of the head was maintained at a pressure in the microtorr region with a small ion pump.

The Source of Oxygen Atoms

In the experiment using discharged oxygen, the source of atoms was a 2,450 MHz discharge maintained at a location 15 to 25 cm from the cavity entrance, and powered by a cylindrical coaxial cavity (11) connected to a Burdick medical diathermy microwave generator. The generator was capable of delivering a continuously variable power of

from zero to 100 watts, and, together with the cavity, produced an electric field high enough to maintain a discharge at pressures from below 100 mtorr to nearly atmospheric pressure.

When ozone was pyrolyzed as a source of oxygen atoms, an oven was placed in the same region as the cavity exciter described above. The oven was constructed of two half-cylindrical heating elements 1.75 in. I. D. by 10 cm length. The ends were closed by split asbestos plates having 15 mm holes to pass the quartz flow tube. After the oven was assembled around the flow tube, the heating elements were wrapped with several layers of asbestos tape and then with several layers of fiberglas tape.

The power for the oven was supplied by a 1000 watt variable autotransformer and adjusted until an optical pyrometer showed the temperature inside the oven to be approximately 1200° C. Nearly all the ozone was dissociated, as was indicated by little accumulation in a liquid nitrogen trap downstream from the cavity entrance.

EXPERIMENTAL PROCEDURE AND DATA REDUCTION

From the discussion of the experimental apparatus, we now turn to a description of the data taking and its reduction.

Experimental Procedure

When data were taken using discharged oxygen, both a static and a flow system were used. Initially, a flow system was used because it provided a better signal-to-noise ratio, since fewer atoms recombined before reaching the cavity. After it was discovered that the data were not reproducible, and that O_2 in the $^1\Delta_g$ state was present in sufficient quantities so that O-atoms were produced by reaction with ozone, a nonflowing system was tried in which the atoms merely diffused from the discharge region into the cavity. It was hoped that the ozone concentration would reach steady state and that the $O_2(^1\Delta_g)$ concentration could be reduced to negligible amounts thereby. The EPR signal of $O_2(^1\Delta_g)$, however, was only slightly diminished, which is consistent with observations made in deexcitation experiments (3). Thus, the use of pyrolysis of ozone was indicated.

After the preparation of a quantity of liquid ozone by the procedure described previously, a large amount of liquid oxygen was made for later evaporation and use as a carrier gas for the ozone. The

liquid oxygen was pumped for five or ten minutes to remove non-condensed impurities and then as the ozone was warmed slightly by partially removing its cold trap, the oxygen was bled in through a metering valve until a desired pressure was reached. At this point, the oven being at full temperature, the spectrometer tuned to the maximum of the O-atom EPR signal, and the signal height large enough to insure that a long decay could be followed, the valve was closed. The recorder then monitored the decay of the oxygen atoms in the coated cavity as a function of time.

Two separate runs were made on different days, both runs starting at a squared pressure, (p^2), of 0.1 $torr^2$. The value of (p^2) was increased in increments of 0.1 $torr^2$ up to a point that reasonable measurement from such data was doubtful. This maximum (p^2) was approximately 1.2 $torr^2$. After making the run upward in (p^2), the system was flushed with O_2 at a higher pressure and the same procedure repeated but with decreasing pressure. By the time of arrival at 0.1 $torr^2$, the liquid was depleted enough to prevent another run.

A third run was started after a liquid ozone preparation which required nearly four hours. This run was similar to the previous two except that the initial (p^2) was 0.05 $torr^2$, increased by 0.1 $torr^2$ up to approximately 1.2 $torr^2$, and back down. At this point it was decided to cease data taking as trouble with leaks in the valve to the

cavity had developed. In order to dispose of the ozone, the oven was left on and the pressure increased to 100 torr by allowing the trap to warm slightly. It was thought that this was a perfectly safe procedure, since Benson and Axworthy (4) had no trouble at pressures below atmospheric at room temperature! However, at this point the ozone detonated, destroying the trap and several meters of glass tubing nearby, which ended the data acquisition. The results of these three runs yielded, for the indicated range of pressures, 138 separate decay curves which appeared to be usable.

Digitization of the Data

In order to get the data from decay curves on a piece of chart paper into a form that a computer could use, they were converted to digital form by the CALMA 302 digitizer at the OSU Computer Center. The digitizer was set to record horizontal, x, and vertical, y, coordinates every 0.01 inches.

Each curve was traced at least twice, in groups of approximately 18 curves. A check on the consistency of the scaling parameters between groups was made by tracing, again at least twice, a minimum of one curve from each of the groups. Three curves at the same pressure, picked for average signal-to-noise and decay time, were digitized ten times each in order to see with what precision one can determine the rate constants from these data.

Computer Program and Subroutines

In order to use the mathematical results of Appendix I together with the digitized data and extract the quantity α from them, the following must be done:

1) determine relative signal heights as a function of time,
2) make provisions for smoothing these data,
3) calculate the initial slopes,
4) calculate the natural logarithm of the relative signal heights as a function of time,
5) calculate the quantities $H_i(t)$,
6) $F_i(t)$,
7) $G_i(t)$,
8) and solve the determinants for A and B.

A FORTRAN program together with several subroutines was written to take the raw digitized data and calculate the relative signal heights and their natural logarithm, compute from the horizontal sensitivity the time coordinates, and provide the options of smoothing, choice of interval between data points, plotting smoothed data on raw data, choice of beginning and ending of data used in computations, and choice of the use of up to seven data points to calculate the initial slope. Subroutines were written to smooth the data, calculate the initial slope, compute the integrals called F(t) and G(t), convert data

from digitized form to a table of relative height vs time, calculate the average deviation for the quantities A and B, and provide the computer reparté for the conversational input.

The subroutine named DIGITCON takes the output of the digitizer unpack program and converts it to the table of y vs x values. The unpack program for the digitizer converts the data stored on the magnetic tape at the digitizer consisting of one record of identification and one record of data, and stores it in a BUFFER where the data are placed on one record consisting of four character words of alternating x and y values. The first two words of the data are 1) the number of records associated with each curve (usually one header and one data record), and 2) the number of words making up the data. The digitizer records both x and y values whenever either has moved the 0.01 inch from the last recording so that often coordinates are repeated. Thus, this subroutine reads the header, reads the data, rejects data pairs in which x has not incremented by one, and stores in the computer's memory the table of y vs x.

Subroutine TALK performs most of the functions of telling the operator when the program is ready for certain data such as the horizontal sensitivity and where to go to get more data.

Subroutine SMOOTH takes the table of y vs x values and at the operator's option, smooths the data as many times as desired. The smoothing routine is a nine point running, weighted average (37) which

calculates the smoothed value for y from the four points both preceding and following the smoothed point.

The subroutine named ISLOPE calculates the slope at the first point from a set of data supplied to it using the formulae given by Milne (31, pp. 96-98), giving the user the choice of from three to seven points from which to compute the slope.

Subroutine INTEG is the subprogram which does the numerical integration required to calculate F(t) and G(t) using Simpson's rule, which is exact to polynomials of fourth order.

The final value of the fitted quantities A and B is assumed to be the best value, since it was calculated using the most data. If the data are representative of the chosen model, then every value of A or B should be the same except for random errors regardless of how many data points are used to compute them. The program DATAFIT computes A and B starting with the first three points and increases by two points until it reaches the last point. Subroutine AVERAGE calculates the average of the absolute value of the difference of each of the intermediate A and B values from the final, or "best" value. This gives a rough estimate of the goodness of fit.

The program DATAFIT was designed to be operated from a teletype under the OS-3 operating system employed by the OSU Computer Center; it cannot be run any other way without extensive modification. This program makes use of a built-in conversational ability

to both guide the user through the calculations and allow him use of many data treatment options such as smoothing, alternation of data points, and plotting[4] of smoothed data on raw data points.

Copies of the program and the subroutines are listed in Appendix III.

Data Handling

After the digitization and unpacking of the tape containing the data, the first data were tested to see the effects of smoothing on computation of the initial slope, the effect of using every other data point and smoothing on the initial slope calculations, and whether hand calculations of the initial slope gave more precise results for A and B. The results of these tests were that calculations of initial slopes from different traces of the same curve using unsmoothed data gave large variations in the initial slope. The calculations compared poorly with manual calculations of the initial slope. Smoothing the data one time gave a more uniform result for the initial slope calculations and were comparable to those done by hand. Further smoothing showed no appreciable improvement, so that all further calculations were done with once smoothed data. The initial slope was calculated using a seven point formula (31).

---

[4]The plotting subroutines were kindly supplied by D. Standley (39).

Instead of using all the data for each decay curve, every other point was used up to a maximum of 75 points, or until the relative height dropped to 0.1, which is approximately two decay constants. Tests showed that this procedure gave the same results within experimental uncertainty as using all the data over the same number of decay constants and used less computer time. The output of this computation scheme is a table of the data and the constants A and B, a sample of which is shown in Tables III and IV. A plot of these data is shown in Figure 16.

TABLE III

Sample of the Computer Output, Part I

25; CURVE 51; TRACE 1; 1.00 SEC/CM; P= .4472 TORR

THERE ARE 241 NONZERO DATA POINTS

THERE ARE 60 NONZERO DATA POINTS

SLI= -0.78142243 HO= 1.000 SEC/CM

T (SEC)	R	LN(R)
0	1.00000	0
.05080	.98250	-0.01765
.10160	.94986	-0.05144
.15240	.90952	-0.09483
.20320	.87327	-0.13551
.25400	.83695	-0.17799
.30480	.80413	-0.21799
.35560	.77552	-0.25422
.40640	.74580	-0.29330
.45720	.71825	-0.33094
.50800	.69009	-0.37094
.55880	.66264	-0.41152
.60960	.63823	-0.44906
.66040	.61396	-0.48782
.71120	.59054	-0.52672
.76200	.56753	-0.56646
.81280	.54481	-0.60733
.86360	.52323	-0.64774
.91440	.50225	-0.68866
.96520	.48234	-0.72911
1.01600	.46470	-0.76637
1.06680	.44723	-0.80468
1.11760	.43026	-0.84337
1.16840	.41368	-0.88266
1.21920	.39695	-0.92395
1.27000	.38195	-0.96247
1.32080	.36823	-0.99906
1.37160	.35511	-1.03533
1.42240	.34338	-1.06893
1.47320	.33171	-1.10349
1.52400	.32024	-1.13869
1.57480	.30985	-1.17167
1.62560	.29955	-1.20549
1.67640	.29000	-1.23787
1.72720	.28000	-1.27297
1.77800	.27000	-1.30933

TABLE IV

Sample of the Computer Output, Part II

T (SEC)	R	LN(R)
1.82880	.26000	-1.34707
1.87960	.25000	-1.38629
1.93040	.24000	-1.42712
1.98120	.23000	-1.46968
2.03200	.22000	-1.51413
2.08280	.20955	-1.56281
2.13360	.19985	-1.61020
2.18440	.19069	-1.65709
2.23520	.18141	-1.70701
2.28600	.17253	-1.75717
2.33680	.16439	-1.80549
2.38760	.15710	-1.85088
2.43840	.15054	-1.89352
2.48920	.14439	-1.93521
2.54000	.13955	-1.96936
2.59080	.13500	-2.00248
2.64160	.13045	-2.03673
2.69240	.12470	-2.08187
2.74320	.11916	-2.12732
2.79400	.11383	-2.17304
2.84480	.10833	-2.22254
2.89560	.10329	-2.27026
2.94640	.10000	-2.30259
2.99720	.09500	-2.35388

AAVE = -0.14192 DEV = .03778

BAVE = .74217 DEV = .01774

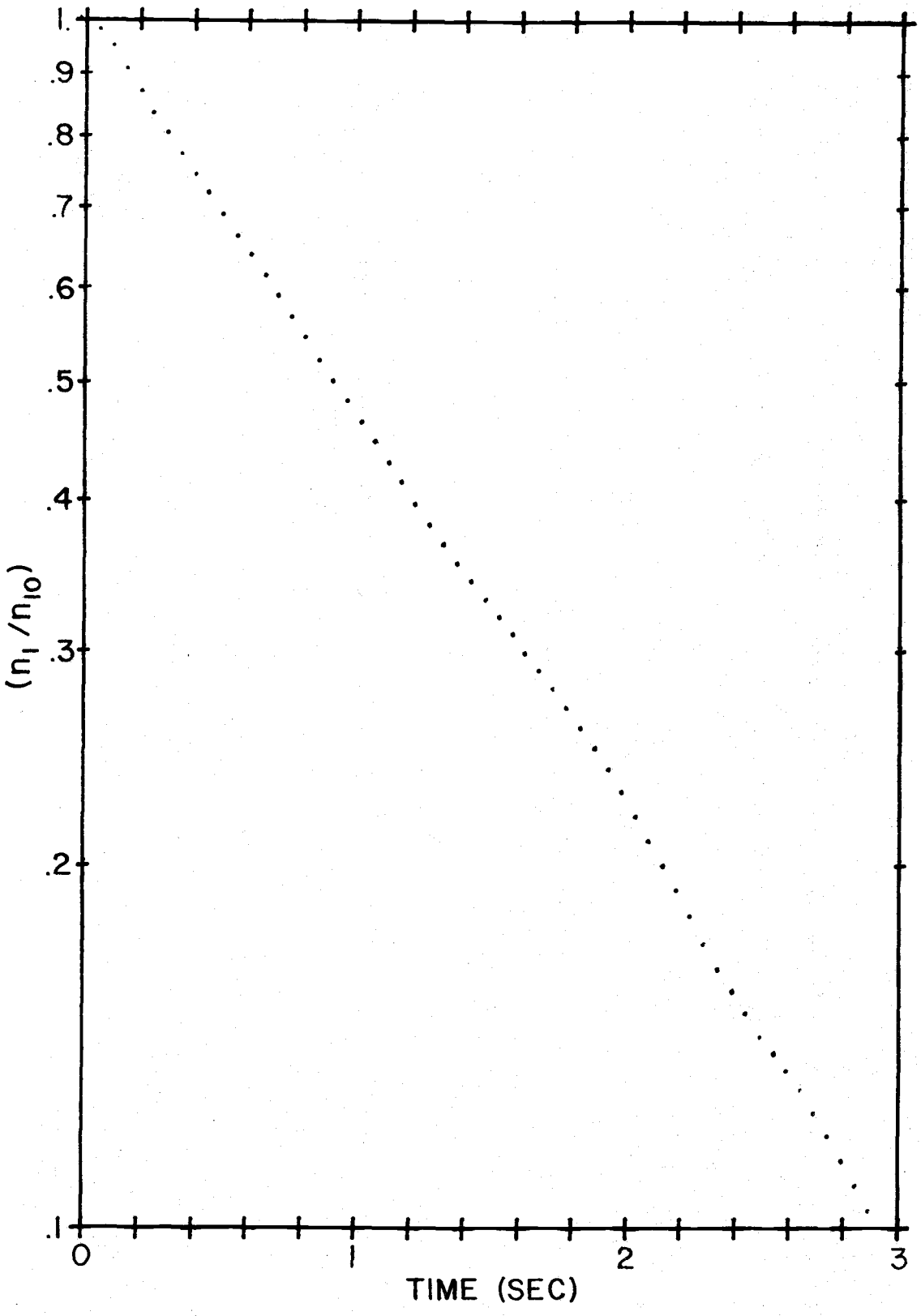

Figure 16. Atomic oxygen decay at .4472 torr.

RESULTS AND DISCUSSION

The output from the computer lists the quantities A and B which will be discussed in this chapter. From the quantity called A defined as $(k_2 n_{10})^{-1}$, the rate constant k_2 cannot be calculated from this experiment, so for the moment, we will consider the quantity B.

Determination of k_1 and k_w

In Appendix I, B is defined as $\alpha = k_w + 2 k_1 n_2^2$, the same as in Equation (5-8). n_2 is defined as the concentration of O_2 molecules, which may be expressed as

$$n_2 = \frac{p_2}{kT}$$

from the ideal gas law. The assumption has been made throughout this work that n_1, $n_3 << n_2$ so that one may approximate the total pressure in the system as p_2. That n_1 is small compared to n_2 was determined by evaluating Equation (4-3) for O and O_2 approximating the integrated intensities by the signal heights. While the concentration of O_3 is less certain, the use of O_2 as a carrier gas reduces the initial fraction of the total pressure which is ozone, and Kaufman and Kelso (23) found that their oven at temperatures in excess of 800° C dissociated nearly all the ozone. Therefore, it is believed that n_3 is also small compared to n_2, and we may write

$$n_2 \doteq \frac{P}{kT} ,$$

where P is the total pressure. In terms of P, α becomes

$$\alpha = k_w + \frac{2 k_1 P^2}{k^2 T^2} , \qquad (7-1)$$

which, when plotted vs P^2, leads to a linear plot with y-intercept k_w and slope $\frac{2 k_1}{k^2 T^2}$. The results, after being edited, are given in Figure 17.

Each curve of raw data was plotted on a semilogarithmic plot to look for irregularities, such as might have been introduced by a leak in the valve. The consequence of a permanent leak is that the decaying signal never can go all the way to zero. Since relative signal heights then are measured from a false zero, the effect is to cause the semilogarithmic plot to fall off faster than an exponential, if one assumes that the time decays are approximately exponential. To see this, let us define h as the true height at time t and h_o as the true initial height. Let δ be the difference between the true zero and the apparent zero. Then, if h' is the apparent height,

$$\frac{h'}{h'_o} = \frac{h + \delta}{h_o + \delta} = \frac{h}{h_o} \frac{(1 + \delta/h)}{(1 + \delta/h_o)} .$$

If we assume that $h/h_o \doteq \exp(-\alpha t)$, then, approximately,

$$\frac{h'}{h'_o} = \frac{\exp(-\alpha t) + \delta/h_o}{1 + \delta/h_o} .$$

A plot of $\ln(h'/h'_o)$ as a function of time is shown in Figure 18, which

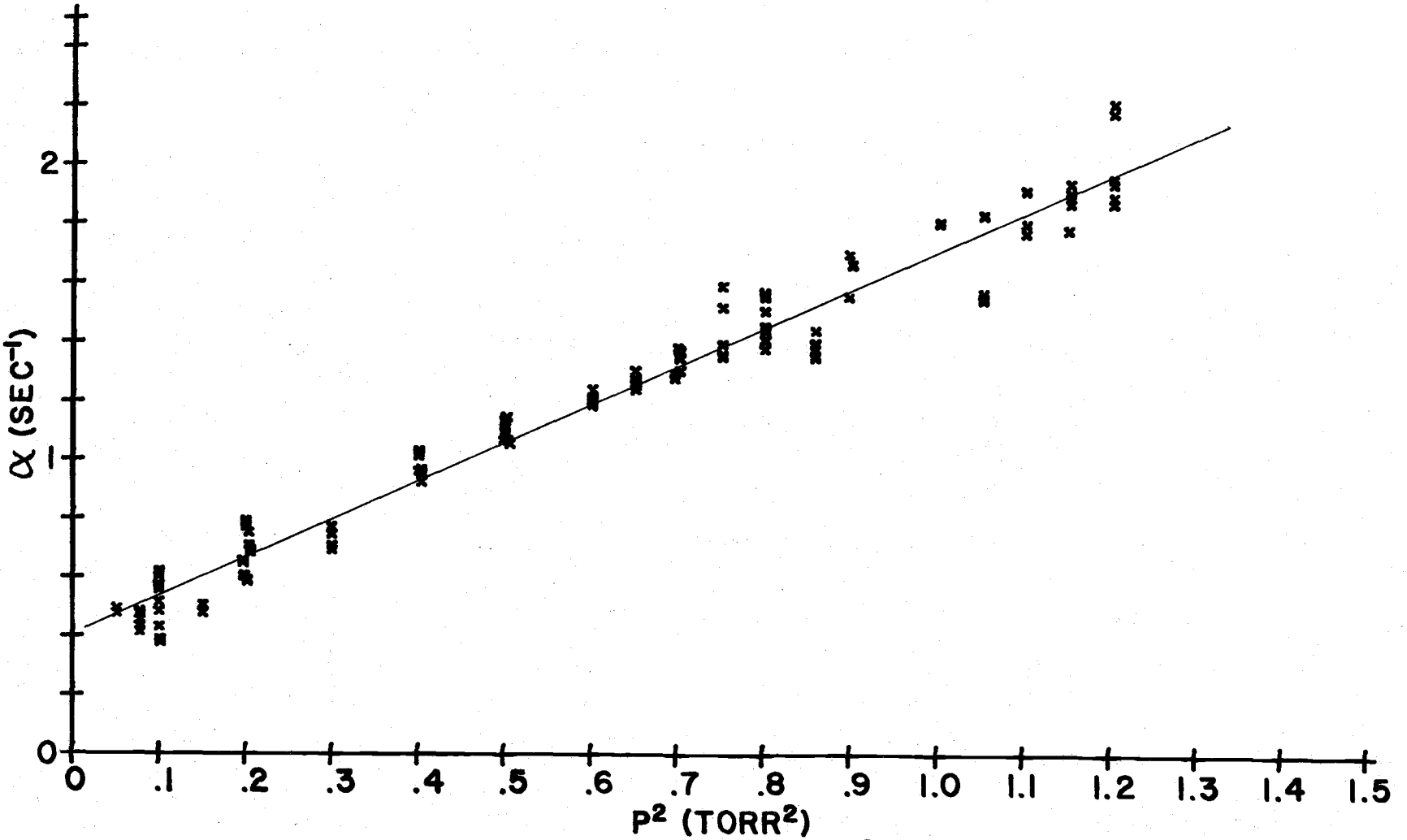

Figure 17. Plot of α vs (p^2).

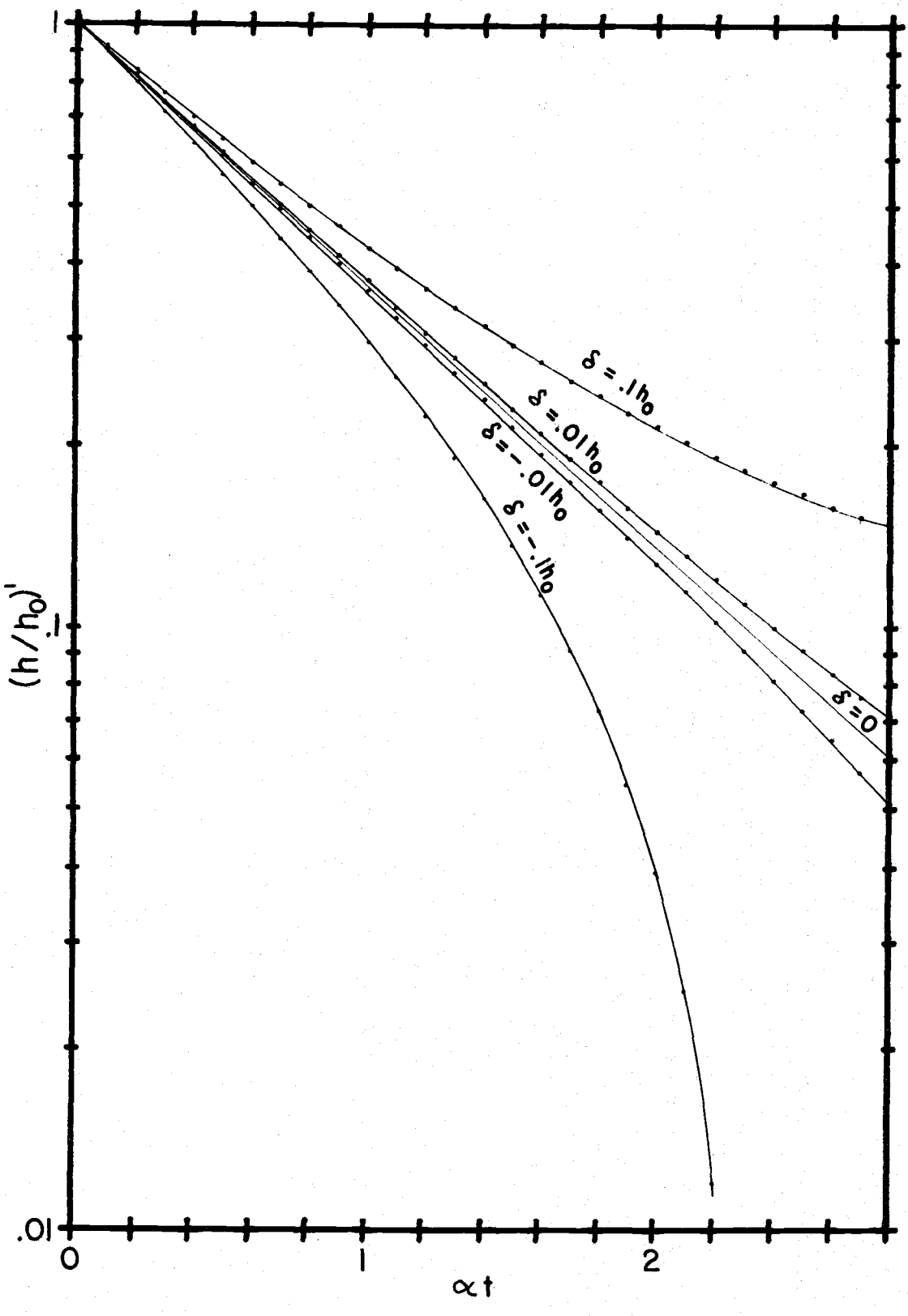

Figure 18. Plot of $\mathrm{Ln}(h/h_o)$ as a function of time.

shows the effect of errors in determining the correct baseline. For the case of a leak, δ is negative and the curve falls off faster than exponential.

A number of curves determined in this experiment showed the behavior described above, and the results of the calculation of α were erratic. The question arises whether such a curve signifies the occurrence of a leak, or whether the initial ozone concentration began far below its steady state value and was building up during the decay. The program will try to find an α, regardless of which case obtains. If the latter case obtains, the value of α should be correct; in the former, however, α may be computed to be anything. In order to remove the possible consequences of leaks, all curves which fell off similar to that shown in Figure 17 were rejected. The remainder of the curves appeared to be very nearly exponential except near the beginning. A few decays that appeared satisfactory yielded values for α which were far from the group of points in Figure 17. These were also rejected.

From the data plotted in Figure 17, a least squares fit for the best straight line was made, which yields a value of $k_w = .41$ and 1.30 for the slope. For the temperature of 300° K, the result of the calculation for k_1 is

$$k_1 = (5.43 \pm .27) \times 10^{-34} \text{ cm}^6 \text{ molecule}^{-2} \text{ sec}^{-1} ,$$

where the uncertainty is the standard error of the slope.

From the value of k_w the wall recombination efficiency γ for fused metaphosphoric acid may be calculated making use of Equation (5-3). For a cylindrical cavity having an inner radius of 10 mm and an internal length of 23.4 mm, neglecting the thickness of the coating, and the volume and the surface of the inlet stem (the volume of the stem is of the order of 0.01 times the volume of the cavity), one finds $\beta = 2.34$. Thus, the recombination efficiency of the fused HPO_3 - $NaPO_3$ mixture is 9.1×10^{-6}.

Determination of the Quantity k_2

The results of the fitting scheme also give the quantity A defined as $(k_2 n_{10})^{-1}$ so that k_2 could be calculated if the initial oxygen atom concentration for each decay were known. There are two reasons why this was not done. In the first place, the quantity A by physical necessity must be positive, yet the program often gave negative values for this quantity which suggests that either the program is in error, or that the fitting scheme is inaccurate for the value A. The program was checked by using it on data generated from Equations (6-9) and (6-10) and the initial conditions for these calculations. The results of these tests were that the fitting program returned the value assumed for the generation of the data very

precisely. The probable cause of the variable results for the parameter A is that the quantity of which A is the coefficient is the least accurately determined of the three functions F(t), G(t), and H(t). Now,

$$H(t) = \mathrm{Ln}(n_1/n_{10}) - \frac{d}{dt}\Big(\mathrm{Ln}(n_1/n_{10})\Big)\Big|_{t=0}\, t$$

is a measure of the departure of the decay from pure exponential behavior, which is small, and depends very strongly upon the measurement of the initial slope. An error in the initial slope can easily change the sign of H(t) and lead to the lack of uniformity in the value of A.

There is yet another difficulty in determining k_2; one must also measure n_{10}, the initial oxygen atom concentration. In principle, this may be readily done from the results of Equation (4-3), which relates concentration and susceptibility,

$$n_1 \sim n_2 \frac{\int_{-\infty}^{\infty} \chi_1'' \, dH}{\int_{-\infty}^{\infty} \chi_2'' \, dH},$$

where n_2 is proportional to the total pressure P. The difficulty lies in measuring $\int_0^{\infty} \chi_1'' \, dH$, since the spectrum of atomic oxygen involves six lines which cannot be resolved sufficiently. Lorentzian lines have the unfortunate characteristic that so much of the area under the curve lies in the tails, that to cut off the integration too soon

causes serious errors in the integral (20). If the lines were well resolved, then one could compensate theoretically for the area remaining beyond the points where the integration is terminated. If one sufficiently modulation-broadens the spectrum so that it appears as one line, then the question arises whether it is truly Lorentzian so that Equation (3-8) is yet valid.

Since k_2 is not determinable from this experiment, it will be estimated from k_1 and the ratio k_2/k_1 determined by Benson and Axworthy (4), and which they give as $1.12 \times 10^{-3} \exp(-6600/kT)$ l/mole for M = O_2 which, at 300° K, gives for k_2:

$$k_2 = 6.12 \times 10^{-15} \text{ cc/molecule sec,}$$

which compares to the value of 4.19×10^{-15} cc/molecule sec from a more recent determination by Benson and Axworthy (5).

Discussion

In order to compare the result of the measurement of k_1 from this experiment, the values of other workers are tabulated in Table V for both discharged oxygen and atomic oxygen produced by dissociation of both ozone and O_2.

The results for k_1 using discharged oxygen listed in Table V show an average of 4.4×10^{-34} cc^2 $molecule^{-2}$ sec^{-1}, which is nearly 20% lower than the average of 5.7×10^{-34} cc^2 $molecule^{-2}$ sec^{-1} for

Table V

Summary of Atomic Oxygen Rate Constants k_1

Method for atom production	k_1 (10^{-34} cc^2 molec^{-2} sec^{-1})	Pressure (torr)	Experimental method	Source
Microwave discharge	2.8	0.1 - 3	isothermal calorimeter	(7)
	6.9	0.8 - 3.4	EPR, flow	(15)
	6.1			(17)
	5.5	0.2 - 1.6	NO titration	(21)
	1.9			(22)
	3.0	≤ 2	NO titration	(25)
Pyrolysis of ozone	3.6	10 - 100	thermal decomposition of ozone	(5)
	4.8	17 - 170	shock pyrolysis of ozone	(19)
	6.5	0.6 - 5.5	NO titration	(24)
	8.8	1 - 8	NO titration	(32)
	3.8	11 - 52	thermal decomposition of ozone	(46)
	5.4	0.2 - 1.1	EPR, static	this work
Photodissociation of O_2	6.4	12 - 20	chemiluminescence	(40)

k_1 obtained using pyrolysis of ozone. The use of the discharge for producing oxygen atoms is known (23) to cause irregularities in the interpretation of recombination data, a fact which is supported by this experiment, and leads to a value of k_1 which is too low. While the conclusion that data acquired from discharged oxygen were not reproducible doesn't demonstrate the presence of metastable species of molecular oxygen, it does reinforce the conclusions of Kaufman and Kelso (23) that the reaction of $O_2(^1\Delta_g)$ state with ozone leads to a k_1 which is too low, and that all results obtained with discharged oxygen are unreliable and should be discarded.

In order to determine the accuracy of the experimental determination of k_1, one must estimate the uncertainties in the slope of the α vs (p^2) plot of Figure 16, the absolute temperature, and the pressure. The fractional uncertainties in the slope, temperature and pressure are approximately ± .015, ±.017, and ±.01 respectively, and these errors propagate in the computation of k_1 to give a 5% error in the determination of that quantity.

The value of 5.43×10^{-34} cc^2 $molecule^{-2}$ sec^{-1} obtained in this experiment for the rate constant k_1 agrees well with nearly all the values of other workers measured from non-discharge sources of oxygen atoms. These are listed in Table V. The determinations from shock tube studies, photodissociation, and the NO titration of Kaufman and Kelso (23) agree within 20%, while the ozone thermal decomposition

studies and the NO titration experiment of Mulcahy and Williams (32) give results for k_1 which differ from these by more than 30%. The experimental determination of k_1 by Mulcahy and Williams may be too high by as much as a factor of two.

The advantages of this experiment are twofold. In the first place the question of ozone concentration is eliminated, and secondly, the reaction may be studied over several decay constants. The result of the study made upon the ozone kinetics is that the equilibrium value is realized only under special conditions if at all; the ozone concentration, if it starts below equilibrium, approaches some steady state value less than equilibrium, and then usually slowly. Because this behavior is masked somewhat by the first-order wall reaction, one cannot be sure of first-order kinetics unless the reaction is followed over several time constants, an accomplishment not possible in flow experiments with tubes of reasonable lengths and flow speeds fast enough to make back diffusion negligible. Thus the data from flow experiments reflect the behavior of the initial time decay and may be interpreted as having a beginning slope of

$$k_w + k_1 n_2^2,$$

only if the initial ozone concentration is zero.

Kaufman and Kelso (23) measure a value of 6.5×10^{-34} cc^2 $molecule^{-2}$ sec^{-1} for k_1, assuming the ozone concentration is negligible,

since their O-atom partial pressures were always of the order of one mtorr. The sensitivity of their ozone detector was approximately 0.1 mtorr which is nearly 10% of the equilibrium concentration of ozone at one torr total pressure. This much difference from zero initial ozone concentration would lead to a value of 5.9×10^{-34} cc^2 $molecule^{-2}$ sec^{-1} for k_1. Thus, it is suggested that the value of k_1 measured by Kaufman and Kelso is an upper limit.

The value of 8.8×10^{-34} cc^2 $molecule^{-2}$ sec^{-1} measured by Mulcahy and Williams (32) is extremely high and is probably due to the fact that they assumed that the ozone concentration was zero when the flow speed was adjusted for a minimum in their pseudo-first-order rate constant, while in fact it probably was at a steady state value determined by the initial ozone concentration. If the flow were such as to permit incomplete dissociation of the ozone and establish a concentration larger than equilibrium, any reduction of ozone from the oven would be compensated for at the expense of the concentration of atomic oxygen, but equilibrium would tend to be maintained, and hence, a constant pseudo-first-order rate constant. If, however, the initial ozone concentration were less than equilibrium, then the reduction of flow speed would establish a new steady state value different from zero and consistent with the oxygen atom concentration. Thus, the value of k_1 determined by these researchers could be as much as half as large as reported.

The result of a photodissociation, CO chemiluminescent determination by Stuhl and Niki (40) in which the ozone reaction with atomic oxygen is neglected entirely is 6.4×10^{-34} cc^2 $molecule^{-2}$ sec^{-1}. The neglect is justified somewhat, since at least half the gas concentration in the reaction vessel is CO.

The reconsideration (5) of their previously published work by Benson and Axworthy (4) on the thermal decomposition of ozone yields for k_1 the value of $8.2 \times 10^{-33} \exp(890/kT)$ cc^2 $molecule^{-2}$ sec^{-1}, which becomes 3.6×10^{-34} cc^2 $molecule^{-2}$ sec^{-1} at 300° K. Zaslowski et al. (46) measure in an experiment similar to that of Benson and Axworthy k_{-1}[5] $1.2 \times 10^{-29} \exp(24,300/kT)$ cc $molecule^{-1}$ sec^{-1} for M = O_3. To calculate $k_{-1}^{O_2}$ one must use the efficiency ratio $k_{-1}^{O_2}/k_{-1}^{O_3}$ which Benson and Axworthy report as .44. This leads to k_{-1} at 300° K of 2.6×10^{-26} cc $molecule^{-1}$ sec^{-1}. The rate constant k_1 may be calculated from the equilibrium constant $K = k_1/k_{-1} = 3.27 \times 10^{-8}$ cc $molecule^{-1}$ (6), which results in a value of 3.8×10^{-34} cc^2 $molecule^{-2}$ sec^{-1} for k_1. A shock tube study for the thermal decomposition of ozone in nitrogen yields (19) $k_{-1}^{N_2} = 9.6 \times 10^{-10} \cdot \exp(-23,150/RT)$ cc $molecule^{-1}$ sec^{-1} when the data of Benson and Axworthy are included. The relative efficiency of O_2 and N_2 (4) is

---

[5] The reaction rate constant k_{-1} denotes the reverse reaction associated with k_1.

1.07 which leads to $k_{-1}^{O_2} = 1.4 \times 10^{-26}$ cc molecule^{-1} sec^{-1}. When k_{-1} is multiplied by K, the equilibrium constant, the result is $k_1^{O_2} = 4.6 \times 10^{-34}$ cc^2 molecule^{-2} sec^{-1}.

It is seen from the experimental results listed above that the results of the thermal decomposition of ozone studies lead to values of k_1 which are quite low: 3.6, 3.8, and 4.6×10^{-34} cc^2 molecule^{-2} sec^{-1}. All these values were calculated from the inverse reaction rate constants and the equilibrium constant K. The heat of formation ΔH_f^o for ozone at 0° K is known to ± 0.4 kcal/mole, which results in an uncertainty of a factor of two in the equilibrium constant K (25, 5). Thus, the results of this experiment are in agreement within the experimental uncertainty with not only the thermal decomposition of ozone experiments, but also the other methods listed in Table V using pyrolysis of ozone. Indeed, some of the results of discharged oxygen experiments are also compatible, which Kaufman and Kelso (23) feel may be caused by hydrogenous impurities compensating for the O-atom production by metastable O_2 reacting with ozone.

The conclusions of this experiment, then, are that the effect of the nonequilibrium of ozone causes much variation in the computations of the rate constant k_1, that discharged oxygen cannot be used as a source of O-atoms unless one finds a way to include the metastable O_2 reaction, and that the measurement of the rate constant $k_1 = 5.43 \times 10^{-34}$ cc^2 molecule^{-2} sec^{-1} is probably the best result to date, since

the need for the knowledge of the ozone concentration has been eliminated from its determination.

BIBLIOGRAPHY

1. Abragam, A. and J. H. Van Vleck, Theory of microwave Zeeman in atomic oxygen. The Physical Review 92:1448-1455. 1953.

2. Amdur, I. and A. L. Robinson. The recombination of hydrogen atoms I. The Journal of the American Chemical Society 55: 1395-1406. 1933.

3. Bader, L. W. and E. A. Ogryzlo. Reactions of $O_2(^1\Delta_g)$ and $O_2(^1\Sigma_g)$. Discussions of the Faraday Society 37:46-56. 1965.

4. Benson, S. W. and A. E. Axworthy. Thermal decomposition of ozone. The Journal of Chemical Physics 26:1719-1726. 1957.

5. Benson, S. W. and A. E. Axworthy. Reconsideration of the rate constants from the thermal decomposition of ozone. The Journal of Chemical Physics 42:2614-2615. 1965.

6. Dow Chemical Corporation, The. JANAF interim thermochemical tables, Vol. II. Midland, Michigan, 1963.

7. Elias, L., E. Ogryzlo, and H. I. Schiff. The study of electrically discharged O_2 by means of an isothermal calorimetric detector. The Canadian Journal of Chemistry 37:1680-1689. 1969.

8. Evenson, K. and D. S. Burch. X band ESR cavity for studies of paramagnetic gases. The Reviews of Scientific Instruments 37: 236-237. 1966.

9. Falick, A. M., B. H. Mahan, and R. J. Myers. Paramagnetic resonance spectrum of the $^1\Delta_g$ oxygen molecule. The Journal of Chemical Physics 42:1837-1838. 1965.

10. Feenberg, E. and G. E. Pake. Notes on the quantum theory of angular momentum. Stanford, California, Stanford University Press, 1959. 56 p.

11. Fehsenfeld, F., K. Evenson, and H. Broida. Microwave discharge cavities operating at 2450 MHz. The Reviews of Scientific Instruments 36:295-298. 1965.

12. Findlay, F. D. and D. R. Snelling. Collisional deactivation of $O_2(^1\Delta_g)$. The Journal of Chemical Physics 55:545-551. 1971.

13. Foner, S. N. and R. L. Hudson. Metastable oxygen molecules produced by electrical discharges. The Journal of Chemical Physics 25:601-602. 1956.

14. Greaves, J. C. and J. W. Linnett. Recombination of atoms at surfaces. Transactions of the Faraday Society 25:1355-1361. 1959.

15. Hacker, D., S. Marshall, and M. Steinberg. Recombination of atomic oxygen on surfaces. The Journal of Chemical Physics 35:1788-1792. 1961.

16. Halbach, K. Modulation-effect corrections for moments of magnetic resonance line shapes. The Physical Review 119:1230-1233. 1960.

17. Harteck, P. and R. R. Reeves Jr. AFOSR-TR-57-50, ASTIA No. AD 136-421. (Cited in: Kaufman, F Reactions of oxygen atoms. In: Progress in Reaction Kinetics, vol. 1. New York, Pergamon, 1961. pp. 1-39.)

18. Herzberg, G. Molecular spectra and molecular structure I. Spectra of diatomic molecules. 2d ed. Princeton, N. J., D. Van Nostrand Company, 1960. 658 p.

19. Jones, W. M. and N. Davidson. The shock pyrolysis of ozone. Abstracts of Papers, 135th Meeting, American Chemical Society: 37R-38R. 1959.

20. Judeikis, H. Errors in the evaluation of moments of a paramagnetic resonance line. The Journal of Applied Physics 35: 2615-2617. 1964.

21. Kaufman, F. Air afterglow and kinetics of some reactions of atomic oxygen. The Journal of Chemical Physics 28:352-353. 1958.

22. Kaufman, F. Reactions of oxygen atoms. In: Progress in reaction kinetics, vol. 1. New York, Pergamon, 1961. pp. 1-39.

23. Kaufman, F. and J. R. Kelso. Rate constant of the reaction $O + O_2 \rightarrow O_3 + O_2$. Discussions of the Faraday Society 37:26-37. 1964.

24. Kaufman, F. and J. R. Kelso. M effect in the gas-phase recombination of O with O_2. The Journal of Chemical Physics 46: 4541-4543. 1967.

25. Kretchmer, C. B. and H. L. Peterson. Recombination kinetics of atomic oxygen at room temperature. The Journal of Chemical Physics 33:948-949. 1960.

26. Krongelb, S. and M. W. P. Strandberg. Use of paramagnetic-resonance techniques in the study of atomic oxygen recombination. The Journal of Chemical Physics 31:1196-1210. 1959.

27. Linnett, J. W. and D. G. H. Marsden. The kinetics of the recombination of oxygen atoms at a glass surface. Proceedings of the Royal Society (London) A234:489-504. 1956.

28. Linnett, J. W. and D. G. H. Marsden. The recombination of oxygen atoms at salt and oxide surfaces. Proceedings of the Royal Society (London) A234:504-515. 1956.

29. Marshall, T. C. Studies of atomic recombination of nitrogen, hydrogen, and oxygen by paramagnetic resonance. The Physics of Fluids 5:743-753. 1962.

30. Miller, T. A. Rotational moment, rotational g-factor, electronic orbital g-factor, and anisotropy of the magnetic susceptibility of $^1\Delta O_2$. The Journal of Chemical Physics 54:330-337. 1971.

31. Milne, W. E. Numerical calculus. 2d ed. Princeton New Jersey, Princeton University Press, 1949. 393 p.

32. Mulcahy, M. F. R. and J. R. Williams. The kinetics of combination of oxygen atoms with oxygen molecules. Discussions of the Faraday Society 64:59-70. 1968.

33. Noxon, J. F. Observation of the ($b^1\Sigma_g^- - a^1\Delta_g$) transitions in O_2. The Canadian Journal of Physics 39:1110-1119. 1961.

34. Pake, G. E. Paramagnetic resonance. New York, W. A. Benjamin, 1962. 205 p.

35. Radford, H. E. and V. W. Hughes. Microwave Zeeman spectrum of atomic oxygen. The Physical Review 114:1274-1279. 1959.

36. Reeves, R. R., G. Mannella, and P. Harteck. The rate of recombination of oxygen atoms. The Journal of Chemical Physics 32:632-633. 1960.

37. Savitzki, A. and M. Golan. Smoothing and differentiation of data by simplified least squares procedures. Analytical Chemistry 36:1627-1639. 1964.

38. Smith, W. V. The surface recombination of H atoms and OH radicals. The Journal of Chemical Physics 11:110-125. 1943.

39. Standley, D., M. S., Research Assistant, Oregon State University, School of Oceanography. Personal Communication. Corvallis, Oregon.

40. Stuhl, F. and H. Niki. Measurements of rate constants for termolecular reactions of $O(^3P)$ with NO, O_2, CO, N_2, and CO_2 using a pulsed vacuum-uv photolysis-chemiluminescent method. The Journal of Chemical Physics 55:3943-3953. 1971.

41. Tinkham, M. and M. W. P. Strandberg. The interaction of molecular oxygen with a magnetic field. The Physical Review 97:951-966. 1955.

42. Van Vleck, J. H. and V. F. Weisskopf. On the shape of collision-broadened lines. The Reviews of Modern Physics 17:227-236. 1945.

43. Wahlquist, H. Modulation broadening of unsaturated Lorentzian lines. The Journal of Chemical Physics 35:1708-1710. 1961.

44. Westenberg, A. A. and N. De Haas. Quantitative measurements of gas phase O and N atom concentrations by ESR. The Journal of Chemical Physics 40:3087-3098. 1965.

45. Williams, F. D. and M. F. R. Mulcahy. The effect of various coatings on the recombination coefficient of oxygen atoms at glass surfaces. The Australian Journal of Chemistry 19:2163-2167. 1966.

46. Zaslowsky, J. A., H. Urbach, F Leighton, R. Wnuk, and J. Wojtowicz. The kinetics of homogeneous gas phase thermal decomposition of ozone. The Journal of the American Chemical Society 82:2682-2686. 1960.

APPENDICES

APPENDIX I

THE SOLUTION OF THE DIFFERENTIAL EQUATIONS

The reactions given by Equations (5-4), (5-5), and (5-6) lead by the Law of Mass Action to the coupled differential equations

$$\frac{dn_1}{dt} = - k_w n_1 - k_1 n_1 n_2^2 - k_2 n_1 n_3 , \tag{I-1}$$

$$\frac{dn_3}{dt} = k_1 n_1 n_2^2 - k_2 n_1 n_3 . \tag{I-2}$$

These equations cannot in general be solved in closed form for either n_1 or n_3, but a solution may be obtained numerically.

If Equation (I-2) is subtracted from Equation (I-1), and the results integrated, a solution for n_3 in terms of n_1 can be obtained as

$$n_3 = n_{30} + n_1 - n_{10} + \alpha \int_0^t n_1 \, d\tau \tag{I-3}$$

where $\alpha = k_w + 2 k_1 n_2^2$. This expression for n_3 may then be substituted into Equation (I-1) to give after some rearrangement

$$\frac{d \mathrm{Ln}\, n_1}{dt} = - k_w - k_1 n_2^2 - k_2 n_{30} - k_2 (n_1 - n_{10})$$

$$- \alpha k_2 \int_0^t n_1 \, d\tau . \tag{I-4}$$

If Equation (I-4) is evaluated at t = 0, then

$$\left.\frac{d\,Ln\,n_1}{dt}\right|_{t=0} = -k_w - k_1 n_2^2 - k_2 n_{30}$$

which when substituted into Equation (I-4) results in

$$\frac{d\,Ln\,n_1}{dt} = \left.\frac{d\,Ln\,n_1}{dt}\right|_{t=0} - k_2(n_1 - n_{10}) - \alpha k_2 \int_0^t n_1\, d\tau . \quad \text{(I-5)}$$

Equation (I-5) may be expressed in terms of n_1 relative to n_{10}. If we define r to be n_1/n_{10}, then we have

$$\frac{d\,Ln\,r}{dt} = \left.\frac{d\,Ln\,r}{dt}\right|_{t=0} - k_2\, n_{10}(r-1) - \alpha k_1\, n_{10} \int_0^t r\, d\tau,$$

which may be formally integrated to yield,

$$Ln\, r = \left.\frac{d\,Ln\,r}{dt}\right|_{t=0} t - k_2\, n_{10} \int_0^t (r-1)\, d\tau$$

$$- \alpha k_1\, n_{10} \int_0^t \int_0^{t'} r\, d\tau d\tau' . \quad \text{(I-6)}$$

The last term of Equation (I-6) can be reduced to a single integral upon performing a partial integration. Consider the double integral of the function f(t),

$$\int_0^t \int_0^{t'} f(t'')\, dt''\, dt' . \quad \text{(I-7)}$$

For the purpose of partial integration, let

$$u = \int_0^{t'} f(t'')\, dt'' , \qquad du = \frac{\partial u}{\partial t'}\, dt' ,$$

$$v = t' , \quad \text{and} \qquad dv = dt' .$$

Thus,

$$\int_0^t \left(\int_0^{t'} f(t'')\, dt'' \right) dt' = t' \int_0^{t'} f(t'')\, dt'' \Big|_0^t - \int_0^t t' \frac{\partial}{\partial t'} \left(\int_0^{t'} f(t'')\, dt'' \right) dt' ,$$

which upon evaluating the first term on the right yields

$$\int_0^t \left(\int_0^{t'} f(t'')\, dt'' \right) dt' = t \int_0^t f(t'')\, dt'' - \int_0^t t' \frac{\partial}{\partial t'} \left(\int_0^{t'} f(t'')\, dt'' \right) dt' .$$

Upon evaluating the second term on the right using the Leibniz rule for differentiating integrals with variable limits, Equation (I-7) becomes

$$\int_0^t \int_0^{t'} f(t'')\, dt''\, dt' = t \int_0^t f(t'')\, dt'' - \int_0^t t'\, f(t')\, dt' .$$

Finally, upon changing the dummy variables of integration, Equation (I-7) is expressed as

$$\int_0^t \int_0^{t'} f(t'')\, dt''\, dt' = \int_0^t (t - t')\, f(t')\, dt' \qquad \text{(I-8)}$$

Thus, Equation (I-6) may be written as

$$\text{Ln } r = \frac{d\text{Ln } r}{dt}\Big|_{t=0} t - k_2 n_{10} \int_0^t (r - 1)\, d\tau - \alpha k_1 n_{10} \int_0^t (t - \tau)\, r\, d\tau , \qquad \text{(I-9)}$$

a formal solution for n_1 relative to n_{10}.

APPENDIX II

THE DETERMINATION OF THE RATE CONSTANTS

Equation (I-8) may be written in the form

$$F(t) = - A\, H(t) - B\, G(t) \qquad \text{(II-1)}$$

where

$$F(t) \equiv \int_0^t (r - 1)\, d\tau ,$$

$$G(t) \equiv \int_0^t (t - \tau)\, r\, d\tau ,$$

$$H(t) \equiv \quad Ln\, r - \left.\frac{d Ln\, r}{dt}\right|_{t=0}^{t} ,$$

$A \equiv 1/k_2\, n_{10}$, and

$B \equiv \alpha = k_w + 2k_1\, n_2^2 .$

Since the purpose of this experiment is to measure the rate constants k_w and k_1 which are contained only in the coefficient B, and since F(t), G(t), and H(t) are determinable from the experimental data, one may find those values of A and B which minimize the square error, ε, between the right and left sides of Equation (II-1). If we define ε as follows

$$\varepsilon \equiv \frac{1}{N} \sum_{i=1}^{N} \left[F_i(t) + A\, H_i(t) + B\, G_i(t) \right]^2 , \qquad \text{(II-2)}$$

then the values of A and B which minimize ε are just those which satisfy $\frac{\partial \varepsilon}{\partial A} = 0$ and $\frac{\partial \varepsilon}{\partial B} = 0$. Thus, we have that

$$\frac{\partial \varepsilon}{\partial A} = \frac{2}{N} \sum_{i=1}^{N} [F_i(t) + A\, H_i(t) + B\, G_i(t)]\, H_i(t) = 0 \qquad \text{(II-3)}$$

$$\frac{\partial \varepsilon}{\partial B} = \frac{2}{N} \sum_{i=1}^{N} [F_i(t) + A\, H_i(t) + B\, G_i(t)]\, G_i(t) = 0\,. \qquad \text{(II-4)}$$

These two equations may be expressed as

$$A \sum_{i=1}^{N} H_i^2(t) + B \sum_{i=1}^{N} H_i(t)\, G_i(t) + \sum_{i=1}^{N} F_i(t)\, H_i(t) = 0 \qquad \text{(II-5)}$$

and

$$A \sum_{i=1}^{N} H_i(t)\, G_i(t) + B \sum_{i=1}^{N} G_i^2(t) + \sum_{i=1}^{N} F_i(t)\, G_i(t) = 0\,, \qquad \text{(II-6)}$$

a system of two independent linear equations in two unknowns which may be solved for A and B. The solutions are expressed by Cramer's rule

$$A = -\frac{\begin{vmatrix} \sum_{i=1}^{N} F_i(t)\, H_i(t) & \sum_{i=1}^{N} G_i(t)\, H_i(t) \\ \sum_{i=1}^{N} F_i(t)\, G_i(t) & \sum_{i=1}^{N} G_i^2(t) \end{vmatrix}}{D}\,,$$

$$B = -\frac{\begin{vmatrix} \sum_{i=1}^{N} H_i^2(t) & \sum_{i=1}^{N} F_i(t)\, H_i(t) \\ \sum_{i=1}^{N} H_i(t)\, G_i(t) & \sum_{i=1}^{N} F_i(t)\, G_i(t) \end{vmatrix}}{D}$$

where

$$D = \begin{vmatrix} \sum_{i=1}^{N} H_i^2(t) & \sum_{i=1}^{N} G_i(t)\, H_i(t) \\ \sum_{i=1}^{N} H_i(t)\, G_i(t) & \sum_{i=1}^{N} G_i^2(t) \end{vmatrix}$$

The computer programming listed in the remaining appendix carries out the above scheme for the determination of A and B.

APPENDIX III

COMPUTER PROGRAM AND SUBROUTINES

```
      PROGRAM DATAFIT
      DIMENSION T(1000),Y(1000),PHI(1000),FI(1000),B(1000,2)
      DIMENSION Y1(1000)
      REAL KKK,J2,MIN
1     ND=1
CCCCC OPTION OF DATA FROM A FILE OR DIGITIZER
800   CALL TALK(0.,KK,1)
      IF(KK.EQ.2HNO)GO TO 803
      CALL TALK(KKK,0,2)
      CALL UNEQUIP (40)
      CALL EQUIP(40,KKK)
      REWIND 40
      DO 20 I=1,3000
      READ(40,10)T(I),Y(I)
10    FORMAT(2(E20.12,1X))
      IF(EOF(40))GO TO 700
      IF(Y(I).LE.0.)GO TO 700
20    NN=I
700   PRINT 701,NN
701   FORMAT(1HO,' THERE ARE',I4,' NONZERO DATA POINTS',/)
      GO TO 11
CCCCC DIGITIZER PART OF OPTION.
803   GO TO(909,910)ND
909   CALL TALK(0.,KLM,3)
      CALL TALK(0.,J1,9)
      CALL TALK(0.,NPLOT,14)
      CALL TALK(0.,K1,5)
      CALL TALK(J2,0,10)
      CALL TALK(0.,NST,4)
      CALL TALK(0.,J4,12)
      IF(K1.EQ.3HYES)ISL=0
      IF(K1.EQ.3HYES)GO TO 21
      CALL TALK(0,K2,15)
      CALL TALK(0.,0,13)
      ISL=TTYIN(3HN =)
21    NIN=TTYIN(4HHOW ,4HMANY,4H DAT,4HA PO,4HINTS,4H?    )
      MIN=TTYIN(4HMIN ,4HVALU,4HE OF,4H Y= )
911   CALL TALK(0.,J3,11)
      IF(J3.EQ.0)GO TO 32
      WRITE(45,2000)J2,NST,J4,ISL,NIN
2000  FORMAT(1H1,10HDATA FROM ,A8,//,13H INTERVAL IS ,I2,//,
     19H SMOOTHED,I2,6H TIMES,//,1H ,I2,15H POINT INITIAL
     25HSLOPE,//,1H ,I3,12H DATA POINTS,///)
      IF(NIN.EQ.0)GO TO 32
910   CALL DIGITCON(T,Y,NN,ND,J1,J2,J3)
      N=NIN
      IF(ND.EQ.0)GO TO 32
CCCCC ENTER HORIZONTAL SENSITIVITY.
11    HO=TTYIN(4HHORI,4HZONT,4HAL S,4HENSI,4HTIVI,4HTY(S,
     14HEC/C,4HM)= )
```

```
      IF(HO.LT.0.)ND=1
      IF(HO.LT.0.)GO TO 911
      HM=HO*.0254
      HM2=HM*HM
      HM6=HM2**3
CCCCC
CCCCC ENTER STARTING TIME.
CCCCC
      TO=TTYIN(4HINIT,4HIAL ,4HTIME,3H = )
      DO 29 I=1,NN
      IF((T(I)*HM-TO).LT.0.)GO TO 29
      LV=I-I/2*2
      IF(LV)23,24
24    IVAL=I+1
      GO TO 28
23    IVAL=I
      GO TO 28
29    CONTINUE
28    DENOM=Y(IVAL)
CCCCC CALCULATE DATA POINTS IF INTERVAL IS GREATER THAN ONE.
      DO 30 I=IVAL,NN,NST
      LL=(I-IVAL+NST)/NST
      T(LL)=(T(I)-T(IVAL))*HM
      Y(LL)=Y(I)/DENOM
      Y1(LL)=Y(LL)
      IF(Y(LL).LT.MIN)GO TO 31
30    CONTINUE
31    WRITE(45,811)LL,MIN
      IF(N.GT.LL)N=LL
811   FORMAT(' THERE ARE ',I4,' NONZERO DATA POINTS GREATER'
     1' THAN ',F6.3,/)
CCCCC INITIATE PLOT OPTION.
      IF(NPLOT.EQ.2HNO)GO TO 603
      CALL PLOTA(Y1,LL)
      CALL PLOTB(Y1,LL)
      CALL PLOTPTS(Y1,LL)
603   CALL SMOOTH(Y,LL,T,J4)
      IF(NPLOT.EQ.2HNO)GO TO 602
      CALL PLOTCURV(Y,LL)
602   CALL UNEQUIP(LUN)
      CALL EQUIP(LUN,SHFILE )
CCCCC BEGIN THE CALCULATIONS.
CCCCC CALCULATE LN(Y).
      DO 40 I=1,LL
      IF(I.GT.N)GO TO 41
      FI(I)=Y(I)-1.
      PHI(I)=ALOG(Y(I))
40    CONTINUE
41    DELTAT=T(2)-T(1)
CCCCC CALCULATE OR ENTER THE INITIAL SLOPE.
```

```
      IF(K1.EQ.2HNO)GO TO 71
      SLI=TTYIN(4HINIT,4HIAL ,4HSLOP,4HE = )
      GO TO 80
71    CALL ISLOPE(PHI,T,SLI,ISL,K2)
      PRINT 90,SLI,HO
80    WRITE(45,90)SLI,HO
90    FORMAT(1X,4HSLI=,F13.8,2X,3HHO=,F6.3,7H SEC/CM,//)
      WRITE(45,1000)((T(I),Y(I),PHI(I)),I=1,N)
1000  FORMAT(1X,3(F8.5,2X))
      L=N-N/2*2
      IF(L)51,60
60    N=N-1
      WRITE(45,70)N
70    FORMAT(1X,4HN = ,I3,'  A NEW VALUE',//)
51    NSKIP=0
      H=SHH=SGGI=SFGI=SFXH=SGIH=0.
      DO 50 K=3,N,2
CCCCC CALCULATE INTEGRALS.
      CALL INTEG(K,T,FI,FX,1)
      CALL INTEG(K,T,Y,GI,2)
      H=PHI(K)-SLI*T(K)
      IF(ABS(H).LT.1.E-3)H=0.
      HH=H*H
      GGI=GI*GI
      FGI=GI*FX
      FXH=FX*H
      GIH=GI*H
      SHH=SHH+HH
      SGGI=SGGI+GGI
      SFGI=SFGI+FGI
      SFXH=SFXH+FXH
      SGIH=SGIH+GIH
      DET=SHH*SGGI-SGIH*SGIH
      CHECK=HM6*1.E-4
      IF(ABS(DET).LT.CHECK)GO TO 33
CCCCC CALCULATE DETERMINANTS.
      ADET=SFGI*SGIH-SFXH*SGGI
      BDET=SGIH*SFXH-SHH*SFGI
      L=(K-1)/2-NSKIP
      B(L,1)=ADET/DET
      B(L,2)=BDET/DET
      GO TO 50
33    WRITE(45,102)
102   FORMAT( ' DET = 0')
      NSKIP=NSKIP+1
50    CONTINUE
      DO 57 I=1,2
      CALL AVERAGE(B(1,I),L,AVE,DEV,B(L,I),2)
      WRITE(45,75)AVE,DEV
75    FORMAT(1X,5HAVE =,F10.5,4X,5HDEV =,F10.5,/)
```

```
57      CONTINUE
        IF(J1.EQ.2HNO.AND.ND.NE.0)GO TO 911
        ND=ND+1
        GO TO 910
32      CALL TALK(0.,MNM,7)
        IF(MNM.EQ.3HYES)GO TO 1
        CALL TALK(0.,MMN,8)
        IF(MMN.EQ.3HYES)GO TO 800
        END
```

```
      SUBROUTINE TALK(KK,K,I)
      REAL KK
      GO TO(1,2,3,4,5,6,7,8,9,10,11,12,13,14,15)I
1     PRINT 101
101   FORMAT(1HO,'ARE YOUR INPUT DATA DIRECTLY FROM A '
     1'FILE? ')
      READ 102,K
102   FORMAT(A4)
      RETURN
2     PRINT 201
201   FORMAT(1HO,'WHAT IS THE NAME OF THE FILE? ')
      READ 202,KK
202   FORMAT(A8)
      RETURN
3     PRINT 301
301   FORMAT(1HO,'IT IS ASSUMED THAT THE DATA ARE FROM '
     1'THE DIGITIZER.',/' IS THIS OK? ')
      READ 302,K
302   FORMAT(A4)
      IF(K.EQ.3HYES)RETURN
      PRINT 303
303   FORMAT(1HO,'THERE ARE NO OTHER CHOICES YET, SO '
     1'YOU BETTER START OVER! ')
      GO TO 1
4     PRINT 401
401   FORMAT(1HO,'HOW LARGE AN INTERVAL DO YOU WANT TO '
     1'READ? ')
      K=TTYIN(3HI =)
      RETURN
5     PRINT 501
501   FORMAT(1HO,'WOULD YOU LIKE TO ENTER THE INITIAL '
     1'SLOPE? ')
      READ 502,K
502   FORMAT(A4)
      RETURN
6     PRINT 601
601   FORMAT(1HO,'WOULD YOU LIKE TO TRY ANOTHER SLOPE? ')
      READ 602,K
602   FORMAT(A4)
      RETURN
7     PRINT 701
701   FORMAT(1HO,'WOULD YOU LIKE TO PROCESS SOME MORE '
     1'DATA? ')
      READ 702,K
702   FORMAT(A4)
      RETURN
8     PRINT 801
801   FORMAT(1HO,'WOULD YOU LIKE TO TRY SMOOTHING? ')
      READ 802,K
802   FORMAT(A4)
```

```
      RETURN
9     PRINT 901
901   FORMAT(1HO,'WOULD YOU LIKE CONTINUOUS DATA '
     1'PROCESSING?')
      READ 902,K
902   FORMAT(A4)
      RETURN
10    PRINT 1001
1001  FORMAT(1HO,'WHAT IS THE NAME OF YOUR DATA FILE?')
      READ 1002,KK
1002  FORMAT(A8)
      RETURN
11    PRINT 1101
1101  FORMAT(1HO,'WHICH RECORD DO YOU WANT TO READ?')
      K=TTYIN(3HN =)
      RETURN
12    PRINT 1201
1201  FORMAT(1HO,'HOW MANY TIMES DO YOU WANT TO SMOOTH?')
      K=TTYIN(3HN =)
      RETURN
13    PRINT 1301
1301  FORMAT(1HO,'HOW MANY POINT DERIVATIVE WOULD YOU '
     1'LIKE TO USE?',/)
      RETURN
14    PRINT 1401
1401  FORMAT(1HO,'WOULD YOU LIKE A PLOT OF SMOOTHED '
     1'DATA ON RAW DATA POINTS?')
      READ 1402, K
1402  FORMAT(A4)
      RETURN
15    PRINT 1501
1501  FORMAT(1HO,'AT WHICH DATA POINT DO YOU WANT TO '
     1'START CALCULATING THE INITIAL SLOPE?')
      K=TTYIN(3HN =)
      RETURN
      END
```

```
      SUBROUTINE DIGITCON(T,Y,JJ,NFILE,NNN,NN,N)
CCC...THIS SUBROUTINE TAKES DATA FROM A BUFFER AND CONVERTS
CCC...IT TO BCD DATA.
      DIMENSION HEAD(10),K(3000),T(1),Y(1)
      REAL NN
      IF(NFILE.NE.1)GO TO 30
      CALL UNEQUIP(41)
      CALL EQUIP(41,NN)
30    IF(NFILE.NE.1.AND.NNN.EQ.3HYES)GO TO 117
      REWIND 41
      IF(N.EQ.0)GO TO 108
      IF(N.EQ.1)GO TO 117
      J=N-1
      DO 13 I=1,J
      CALL SEFF(41)
13    CONTINUE
117   BUFFER IN(41,1)(HEAD(1),HEAD(10))
100   GO TO(100,101,102,)UNITSTF(41)
101   PRINT 1061,HEAD
      WRITE(45,106)HEAD
106   FORMAT(1H1,10A8,/)
1061  FORMAT(1H0,10A8,/)
200   BUFFER IN(41,1)(K(1),K(3000))
109   GO TO(109,110,111)UNITSTF(41)
110   NPT=K(2)
      CALL SEFF(41)
      XP=-1.
      NSKIP=0
      DO 115 J=4,NPT,2
      I=(J-2)/2-NSKIP
      T(I)=1.*K(J-1)
      Y(I)=1.*K(J)
      IF(Y(I).LE.0.)GO TO 14
      NSKIP=NSKIP+1
      XP=T(I)
      JJ=I
115   CONTINUE
14    WRITE(45,700)JJ
700   FORMAT(1H0,' THERE ARE 'I4,' NONZERO DATA POINTS',/)
      GO TO 103
102   PRINT 113
113   FORMAT(1H0,' EOF IN HEADING!')
      GO TO 200
111   PRINT 118
118   FORMAT(1H0,' EOF IN THE DATA!')
      PRINT 119
119   FORMAT(1H0,' THE LAST DATA HAVE BEEN PROCESSED.')
108   NFILE=0
103   RETURN
      END
```

```
      SUBROUTINE ISLOPE(PHI,T,SLI,N,K)
      DIMENSION PHI(1),T(1)
      D=T(K+1)-T(K)
11    GO TO(20,30,40,50,60,70,80,90)N
20    PRINT 13
13    FORMAT(' THIS IS AN IMPOSSIBLE CHOICE, TRY AGAIN!',/)
      N=TTYIN(3HN =)
      GO TO 11
30    PRINT 100
100   FORMAT(' THIS IS NOT A VERY ACCURATE CHOICE,TRY AGAIN!
     1',/)
      N=TTYIN(3HN =)
      GO TO 11
40    SLI=(-3.*PHI(K)+4.*PHI(K+1)-PHI(K+2))/(2.*D)
      RETURN
50    SLI=(-11.*PHI(K)+18.*PHI(K+1)-9.*PHI(K+2)+2.*PHI
     1(K+3))/(6.*D)
      RETURN
60    SLI=(-25.*PHI(K)+48.*PHI(K+1)-36.*PHI(K+2)+16.*P
     1HI(K+3)-3.*PHI(K+4))/(12.*D)
      RETURN
70    SLI=(-137.*PHI(K)+300.*PHI(K+1)-300.*PHI(K+2)+20
     10.*PHI(K+3)-75.*PHI(K+4)+12.*PHI(K+5))/(60.*D)
      RETURN
80    SLI=(-147.*PHI(K)+360.*PHI(K+1)-450.*PHI(K+2)+40
     20.*PHI(K+3)
     1-225.*PHI(K+4)+72.*PHI(K+5)-10.*PHI(K+6))/(60.*D)
      RETURN
90    PRINT 12
12    FORMAT(' YOU HAVE EXCEEDED THE NUMBER OF CHOICES,'/
     1' THEREFORE YOU ARE A DOLT!--TRY AGAIN!',/)
      N=TTYIN(3HN =)
      GO TO 11
      END
```

```
      SUBROUTINE SMOOTH(Y,K,T,N)
      DIMENSION Y(1),Q(1500),T(1)
      IF(N.EQ.0)RETURN
      DEL=T(3)-T(2)
      DO 20 J=1,N
      DO 10 I=5,K
10    Q(I)=(-21.*Y(I-4)+14.*Y(I-3)+39.*Y(I-2)+54.*Y(I-1)
     1+59.*Y(I)+54.*Y(I+1)+39.*Y(I+2)+14.*Y(I+3)-21.*Y(I
     2+4))/231.
      Q(1)=Y(1)
      Q(2)=(Y(1)+4.*Y(2)+Y(3))/6.
      Q(3)=(-3.*Y(1)+12.*Y(2)+17.*Y(3)+12.*Y(4)-3.*Y(5))/35.
      Q(4)=(-2.*Y(1)+3.*Y(2)+6.*Y(3)+7.*Y(4)+6.*Y(5)+3.
     1*Y(6)-2.*Y(7))/21.
      Q(K-3)=(-2.*Y(K-6)+3.*Y(K-5)+6.*Y(K-4)+7.*Y(K-3)+
     16.*Y(K-2)+3.*Y(K-1)-2.*Y(K))/21.
      Q(K-2)=(-3.*Y(K-4)+12.*Y(K-3)+17.*Y(K-2)+12.*Y(K
     1-1)-3.*Y(K))/35.
      Q(K-1)=(Y(K-2)+4.*Y(K-1)+Y(K))/6.
      Q(K)=Y(K)
      DO 20 I=1,K
20    Y(I)=Q(I)
      RETURN
      END
```

```
      SUBROUTINE AVERAGE( F,N,AVE,AVEDEV,VAL,K)
CCCCC.TO  FIND  THE AVERAGE AND THE AVERAGE DEVIATION  FROM
CCCCC.THE AVERAGE,  SET K=1.
CCCCC.TO  FIND  THE AVERAGE DEVIATION  FROM  SOME VALUE,
CCCCC.SET K=2 AND THE VALUE IN VAL.
      DIMENSION  F(1)
      SUM=DEV=0.0
      DO  10  I=1,N
10    SUM=SUM+F(I)
      RN=N
      AVE=SUM/RN
      IF(K.EQ.2)AVE=VAL
      DO  20  I=1,N
      ADEV=ABS(AVE-F(I))
20    DEV=DEV+ADEV
      AVEDEV=DEV/RN
      RETURN
      END
```

```
      SUBROUTINE INTEG(K,T,F,FR,IN)
      DIMENSION T(1),F(1)
      D=(T(2)-T(1))/3.
      GO TO(50,60)IN
50    FR=0.
      DO 10 M=3,K,2
10    FR=FR+(F(M-2)+4.*F(M-1)+F(M))*D
      RETURN
60    FR=0.
      DO 30 L=3,K,2
30    FR=FR+((T(K)-T(L-2))*F(L-2)+4.*(T(K)-T(L-1))*F(L-1)
     1+(T(K)-T(L))*F(L))*D
      RETURN
      END
```

```
      SUBROUTINE PLOTA(YY,L)
C****  YY IS THE ORDINATE TO BE PLOTTED
C****  L IS THE NUMBER OF POINTS TO BE PLOTTED
      DIMENSION YY(1),ABCD(6),IABC(3),COMMENT(10)
      INTEGER PENUP,PENDOWN
      EQUIVALENCE (ABCD(5),IABC),(TTMM,IABC(2))
      PENUP=3
      PENDOWN=2
      XORG=2. $YORG=14.
      DO 1 I=1,6
1     ABCD(I)=8H
      ABCD(1)=8H...HOGAN
      CALL DATE(ABCD(4))
      CALL TIME(TTMM)
      IZ=4H    0
      LUN=TTYIN(4HPLOT,4H LUN,3H = )
      RETURN
C**** INITIALIZE PLOTTER AND LABEL IT
      ENTRY PLOTB
      CALL PLOTINT(XORG,YORG,LUN)
      CALL PLOTSYMB(0.,-12.,.21,ABCD,0.,44)
      WRITE(61,100)
100   FORMAT(' ENTER PLOT LABEL --- UP TO 80 CHARS')
      READ(60,101)COMMENT
101   FORMAT(10A8)
C**** REMOVE MISTAKES IF ANY
      CALL CANCEL(COMMENT)
C**** PLOT LABEL
      CALL PLOTSYMB(2.,.5,.14,COMMENT,0.,80)
C**** DRAW AND LABEL Y AXIS
      CALL PLOT(0.,0.,PENUP)
      CALL PLOTSYMB(-.28,0.,.07,IZ,0.,4)
      CALL PLOT(0.,0.,PENUP)
      Y=0.
      DO 2 I=1,4
      Y=Y-.2
      CALL PLOTSYMB(0.,Y,.05,13,90.,-2)
      CALL PLOT(0.,0.,PENUP)
2     CONTINUE
      CALL PLOT(0.,0.,PENUP)
      YJ=0.
      DO 3 I=1,5
      Y=-I
      CALL PLOTSYMB(0.,Y,.10,13,90.,-2)
      YJ=YJ-1.
      ENCODE(4,102,LABEL)YJ
102   FORMAT(F4.2)
      CALL PLOTSYMB(-.35,Y,.07,LABEL,0.,4)
      CALL PLOT(0.,Y,PENUP)
C**** SMALL TICKS
```

```
      IF(I.EQ.5)GO TO 3
      DO 3 II=1,4
      Y=Y-.2
      CALL PLOTSYMB(0.,Y,.05,13,90.,-2)
      CALL PLOT(0.,Y,PENUP)
3     CONTINUE
C**** BORDERS
      CALL PLOT(0.,-5.,PENUP)
      CALL PLOT(7.,-5.,PENDOWN)
      CALL PLOT(7.,0.,PENDOWN)
C**** X-AXIS
      CALL PLOT(0.,0.,PENUP)
      X=0.
      DO 4 I=1,4
      X=X+.2
      CALL PLOTSYMB(X,0.,.05,13,0.,-2)
      CALL PLOT(X,0.,PENUP)
4     CONTINUE
      CALL PLOT(0.,0.,PENUP)
      DO 5 I=1,7
      X=I
      CALL PLOTSYMB(X,0.,.10,13,0.,-2)
      J=10*I
      ENCODE(3,103,LABEL)J
103   FORMAT(I3)
      CALL PLOTSYMB(X-.03,.1,.07,LABEL,0.,3)
      CALL PLOT(X,0.,PENUP)
C**** SMALL TICKS
      IF(I.EQ.7)GO TO 5
      DO 5 II=1,4
      X=X+.2
      CALL PLOTSYMB(X,0.,.05,13,0.,-2)
      CALL PLOT(X,0.,PENUP)
5     CONTINUE
C**** GO BACK TO ORIGIN
      CALL PLOT(0.,0.,PENUP)
      RETURN
      ENTRY PLOTPTS
C**** PLOT THE POINTS
      K=L
      IF(K.GT.70)K=70
      X=0.
      DO 10 I=1,K
      X=X+.1
      CALL PLOTSYMB(X,2.*YY(I),.05,4,0.,-1
10    CONTINUE
      CALL PLOT(0.,2.*YY(1),PENUP)
      RETURN
C**** PLOT THE CURVE
      ENTRY PLOTCURV
```

```
      K=L
      IF(K.GT.70)K=70
      CALL PLOT(.1,2.*YY(1),PENUP)
      X=0.
      DO 20 I=1,K
      X=X+.1
      CALL PLOT(X,2.*YY(I),PENDOWN)
20    CONTINUE
C**** END OF PLOT ****
      CALL PLOT(-2.,6.,-3)
      RETURN
      END
```